Plan-form evolution of drainage basins in response to tectonic changes: Insights from experimental and numerical landscapes

Habousha Kobi[1], Goren Liran[2], Nativ Ron[2], and Gruber Chen[3]

[1]Department of Earth and Environmental Sciences, Ben Gurion University of the Negev, Beer Sheva 84105, Israel.
[2]Ben Gurion University of the Negev
[3]Vanderbilt University

November 16, 2022

Abstract

Spatial gradients in rock uplift control the relief and slope distribution in uplifted terrains. Relief and slopes, in turn, promote channelization and fluvial incision. Consequently, the geometry of drainage basins is linked to the spatial pattern of uplift. When the uplift pattern changes basin geometry is expected to change via migrating water divides. However, the relations between drainage pattern and changing uplift patterns remain elusive. The current study investigates the plan-view evolution of drainage basins and the reorganization of drainage networks in response to changes in the spatial pattern of uplift, focusing on basin interactions that produce globally observed geometrical scaling relations. We combine landscape evolution experiment and simulations to explore a double-stage scenario: emergence of a fluvial network under block uplift conditions, followed by tilting that forces drainage reorganization. We find that the globally observed basin spacing ratio and Hack's parameters emerge early in basin formation and are maintained by differential basin growth. In response to tilting, main divide migration induces basins' size changes. However, basins' scaling relations are mostly preserved within a narrow range of values, assisted by incorporation and disconnection of basins to and from the migrating main divide. Lastly, owing to similarities in landscape dynamics and response rate to uplift pattern changes between experiment and simulations, we conclude that the stream power incision model can represent fluvial erosion processes operating in experimental settings.

Hosted file

agu_suppinfo.docx available at https://authorea.com/users/524177/articles/595409-plan-form-evolution-of-drainage-basins-in-response-to-tectonic-changes-insights-from-experimental-and-numerical-landscapes

Hosted file

essoar.10512204.1.docx available at https://authorea.com/users/524177/articles/595409-plan-form-evolution-of-drainage-basins-in-response-to-tectonic-changes-insights-from-experimental-and-numerical-landscapes

Plan-form evolution of drainage basins in response to tectonic changes: Insights from experimental and numerical landscapes

K. Habousha[1], L. Goren[1], R. Nativ[1,2,3] and C. Gruber[4].

[1]Department of Earth and Environmental Sciences, Ben Gurion University of the Negev, Beer Sheva 84105, Israel.

[2]Helmholtz Centre Potsdam, GFZ German Research Centre for Geosciences, Potsdam, Germany

[3]Institute of Earth and Environmental Science, University of Potsdam, Potsdam, Germany

[4]Department of Civil and Environmental Engineering, Vanderbilt University, Nashville, TN 37215, USA.

Corresponding author: Kobi Habousha (kobihavu@gmail.com)

Key points

- A new experimental apparatus is used to study plan-form changes of drainage basins in response to tectonic tilting.
- Regularity in basin geometrical scaling is a fundamental feature of juvenile basins and is preserved during reorganization.
- Tectonic tilting triggers reorganization that changes basin size but maintains geometrical scaling relations within a narrow range.

Abstract

Spatial gradients in rock uplift control the relief and slope distribution in uplifted terrains. Relief and slopes, in turn, promote channelization and fluvial incision. Consequently, the geometry of drainage basins is linked to the spatial pattern of uplift. When the uplift pattern changes basin geometry is expected to change via migrating water divides. However, the relations between drainage pattern and changing uplift patterns remain elusive. The current study investigates the plan-view evolution of drainage basins and the reorganization of drainage networks in response to changes in the spatial pattern of uplift, focusing on basin interactions that produce globally observed geometrical scaling relations. We combine landscape evolution experiment and simulations to explore a double-stage scenario: emergence of a fluvial network under block uplift conditions, followed by tilting that forces drainage reorganization. We find that the globally observed basin spacing ratio and Hack's parameters emerge early in basin formation and are maintained by differential basin growth. In response to tilting, main divide migration induces basins' size changes. However, basins' scaling relations are mostly preserved within a narrow range of values, assisted by incorporation and disconnection of basins to and from the migrating main divide. Lastly, owing to similarities in landscape dynamics and response rate to uplift pattern changes between experiment and simulations, we conclude that the stream power incision model can represent fluvial erosion processes operating in experimental settings.

Plain Language Summary

Mountainous landscapes develop in response to rock uplift that generates high slopes and promotes erosion in river channels. Channels are organized in drainage basins, whose geometry is defined by water divides surrounding them. A surprising feature of drainage basins is that in many cases they show similar geometric properties despite the significant variability in rock uplift pattern that drives basin evolution. The relation between this regularity and changing rock uplift settings remains little explored. In the current study, we explore trends and processes of changes in basin geometry in response to changes in uplift patterns. We use a novel approach for landscape evolution experiments capable of inducing spatial gradients in uplift rate, combined with landscape evolution simulations. We explore a scenario in which

basins form under uniform uplift conditions and then respond to a change in uplift pattern. We find that the globally observed geometric features are fundamental in juvenile basins. Basins' geometry is largely preserved during changes in uplift patterns, assisted by incorporation and disconnection of basins to and from the main water divide. Moreover, similarities between basin evolution in physical and numerical models indicate that simple river erosion models can well represent processes acting on experimental fluvial landscapes.

1. Introduction

Rock uplift emerging from tectonic, isostatic, and mantle dynamic processes is a fundamental force that acts on the Earth's surface and generates topographic gradients that promote fluvial erosion (e.g., Burbank et al., 1996; Howard et al., 1994). The spatial patterns of rock uplift control the magnitude and orientation of topographic gradients, which in turn, dictate the direction of water flow and the organization of fluvial channels in drainage basins (e.g., Forte et al., 2015; Beeson & McCoy, 2020). Consequently, to maintain the links between uplift pattern and drainage pattern, changes in uplift gradients are expected to induce changes in basins' shape and size via fluvial reorganization processes (Davis, 1899; Bishop, 1995). Over geological timescales, uplifted terrains experience spatially and temporally variable patterns of rock uplift, significant changes in the planform geometry of drainage networks and basins should be expected during their evolution (e.g., Willett et al., 2014).

Contrary to this expectation, global analysis of fluvial landscapes show that drainage basins commonly share geometric properties regardless of their tectonic setting and history (e.g., Hack, 1957; Montgomery & Dietrich, 1992; Hovius, 1996; Talling et al. 1997; Willemin, 2000; Walcott & Summerfield, 2009; Purdie & Brook, 2006; Densmore et al., 2005). These geometric properties can be quantitively described using geometrical and topological scaling relations (Horton, 1945; Hack, 1957; Strahler, 1964; Shreve, 1966; Hovius, 1996; Walcott & Summerfield, 2009). For example, Hack's law (Hack, 1957) predicts that the relationship between the mainstream length (L) and its corresponding drainage area (A) follows a power-law relation, $L = cA^h$ where c and h are referred to as Hack's coefficient and exponent, respectively. These two parameters are commonly reported in natural landscapes to be within a relatively narrow range of $1.1 \leq c \leq 4.5$ and $0.45 \leq h \leq 0.67$ (e.g., Mongtomery & Dietrich, 1992; Mueller, 1973; Willemin, 2000; Dodds & Rothman, 2000; Castelltort et al., 2009; Shen et al., 2017; Sassolas-Serrayat et al., 2018). In addition, in linear mountain ranges and faulted blocks, the distance between drainage basins' outlets (S) has been shown to scale linearly with the distance between the main divide and the mountain front (W), such that $R = \frac{W}{S}$, referred to as the spacing ratio (Hovius, 1996; Talling et al., 1997), is approximately constant. In linear converging mountain ranges, R was found to be $1.91 \leq R \leq 2.23$ with an average value of 2.1 (Hovius, 1996). In fault-bounded blocks, R was found to have a slightly broader range of $1.4 \leq R \leq 4.1$ with an average value of 2.5 (Talling, 1997; Purdie & Brook, 2006). Notably, in some rare cases, measured scaling relations are found to deviate from these ranges. For example, Beeson et al. (2016) showed that in the High Plains, located to the east of the Rocky Mountains, and in the Northern Sierra Nevada, United States, nested basins that do not drain the main divide are characterized by anomalous Hack's parameters that fall out of the globally observed range. Walcott and Summerfield (2009) showed that several main basins in the Western and Central Himalayas that likely experienced localized tectonic deformation do not preserve the regular spacing ratio.

The documented regularity of the geometrical scaling relations across various landscapes is surprising since high elevation terrains across the globe experience variable tectonic histories, and because different terrains represent different evolutionary stages. Particularly, some basins dissect recently uplifted regions, while others drain old and tectonically inactive mountain ranges (Montgomery & Brandon, 2002; Matmon et al., 2003; Cox et al., 2010). Presumably, this means that geometric regularity is maintained during, and in spite of, dynamic planform landscape evolution. We therefore hypothesize that reorganization processes arising from changing rock uplift patterns and resulting in changing basin geometry also act in a way that mostly preserves basins' geometrical scaling relations.

Previous studies of landscape evolution explored processes by which geometric regularity, reflected by the spacing ratio, is dynamically maintained under different tectonic, lithologic, and climatic conditions. For example, Talling et al. (1997) proposed that in the early evolutionary stages of uplifted blocks, the scaling relations are preserved via sideways expansion by stream captures in parallel to gradual extension toward the center of the domain. This process was also documented numerically by Giachetta et al. (2014). Based on numerical simulations, Castelltort and Simpson (2006) and Capolongo et al. (2011) showed that in a widening mountain front, basins' geometrical scaling relations are preserved by incorporating new sections of the drainage network that emerged on an initially undissected surface. Giachetta et al. (2014) further explored numerical landscape response to an application of erodibility gradient, and found that during main divide migration toward the lower erodibility side, the geometrical scaling relations were maintained by lateral growth of nested basins on the lower erodibility side, and growth of main basins on the higher erodibility side. Bonnet (2009) demonstrated experimentally that basins' geometrical scaling relations are maintained during main divide migration induced by climatic gradients via shrinking and splitting of basins on the drier side of the landscape.

In this study we explore the dynamic links between changing patterns of rock uplift, the resultant changes in basins shape and size by reorganization processes, and the associated evolution of basins' geometrical scaling relations. A combination of landscape evolution laboratory experiment and numerical simulations was performed to study two dynamical settings: terrains emerging from a subdued topography in response to uniform uplift, followed by an uplift gradient in the form of tilting. We focus on tectonic tilting because (i) tilting is widely-documented in various tectonic settings (e.g., Farías et al., 2005; Jackson et al., 1998; Shikakura et al., 2011; Whittaker et al., 2008; Castelltort et al., 2012; He et al., 2019;

Su et al., 2020; Stewart, 1980; Densmore et al., 2005; Ellis et al., 1999; Stockli et al., 2003), and (ii) previous studies have shown that tectonic tilting induces main divide migration that changes basins' geometry (e.g., Willett et al., 2014; Goren et al., 2014; Whipple et al., 2017; Forte et al., 2015; He et al., 2019, 2021; Shi et al., 2021; Shikakura et al., 2012).

2. Methods

To study drainage basins' geometric evolution under changing uplift patterns, we combined landscape evolution experiments, using a landscape evolution physical apparatus (DULAB; see below) and landscape evolution simulations, using a landscape evolution numerical model (DAC; see below) (e.g., Goren et al., 2014).

2.1. DULAB (Differential Uplift LAndscape-evolution Box)

DULAB is an experimental apparatus for landscape evolution at the mountain-range scale. It is designed to explore the evolution of fluvial systems in response to precipitation-induced surface runoff and uplift with respect to fixed base-level edges (e.g., Crave et al., 2000; Hasbargen & Paola, 2000; Bonnet & Crave, 2003). DULAB is unique in its ability to impose time-variable spatial gradients in uplift rate, allowing it to simulate fluvial system response to changing tectonic gradients.

2.1.1 Experimental setup

DULAB is made of a plexiglass frame with dimensions of 90 (length) x 50 (width) x 35 (height) cm^3, in which the experimental material is initially placed (Figure 1a). The base of the frame consists of six prisms covered by a rubber sheet (by "Four D Rubber Co. Ltd.") sustaining extensional strains as high as 800%. The prisms are mounted on six electrical car jacks connected to power supply units (by "Aim and Thurlby Thandar Instruments") and monitored by a programable controller. Each car jack can be uplifted independently at a time-dependent rate. The car jacks do not uplift continuously but in discrete pulses (0.2 to 0.4 mm per pulse), producing the target uplift rate of each prism as a time average. During an experiment, the experimental material is uplifted and eroded, while the upper edge of the stationary plexiglass frame acts as the base level of the evolving drainage system. The duration of an experiment is limited by the maximum height of the jacks, which is 28 cm.

When spatially uniform uplift is applied, the car jacks are set to uplift at the same rate, and the prisms are uplifted as if they are a single unit. When the car jacks are programmed to uplift differentially, the prisms are uplifted to form a step-like geometry, smoothened by the overlying rubber (Figure 1b). Consequently, the differential uplift pattern is transmitted to the surface of the experimental material according to the 3D geometry of the rubber, as depicted in the side-view section in Figure 1b. The particular geometry for the differential uplift experiment reported here was verified in an earlier calibration stage in which differential uplift was imposed without applying precipitation. Under these conditions, the surface topography, that did not erode by runoff and only slightly deformed by gravitational processes, was observed to be sub-parallel to the topography of the rubber (Figure 1b). To prevent downward deflection of the rubber by the weight of the experimental material and to ensure a linear uplift gradient, three free-to-rotate rigid plates were placed upon the rubber (Figure 1b).

The experimental material constitutes a mixture of 80.5% crushed silica grains ("silica powder"), with a median grain diameter of 75 μm and 19.5% water. The choice of material and specific mixture percentages was informed by previous studies (Crave et al., 2000; Hasbargen & Paola, 2000; Reitano et al., 2020; Bata et al., 2006). These studies demonstrated that saturated ground silica requires only small shear stresses to experience surface erosion, and at the same time is capable of sustaining high slopes for long periods, overall producing realistic landscape features (Reitano et al., 2020; Graveleau et al., 2011; Paola et al., 2009; Bonnet et al., 2006; Crave et al., 2000; Hasbargen & Paola 2000).

For the precipitation system, we used 24 equally spaced sprinklers connected to a pressure valve, mounted approximately one meter above the plexiglass frame. The sprinklers generate precipitation in the form of fine drizzle (with a droplet size of approximately 100μm). The small droplets generate a dense mist that descends upon the experimental surface, leading to surface erosion by water runoff. Material detachment due to droplet impacts ("rain-splash" effect) (e.g., Sweeney et al., 2015) was not detected, and hillslope-like processes were not observed as channelization reached very close to the water divides.

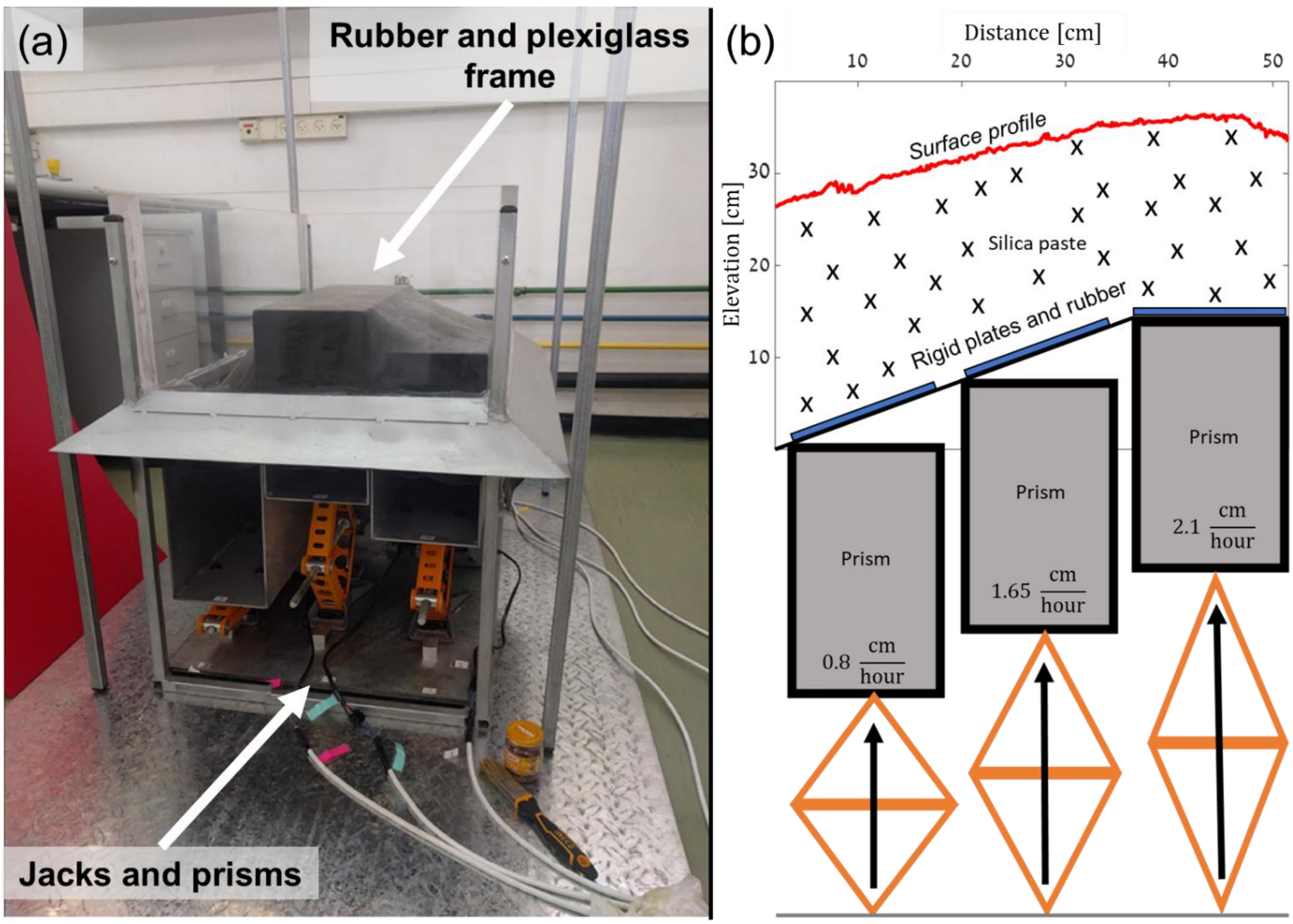

Figure 1: (a) The uplift system of DULAB. Six independent prisms mounted on electrical car jacks under a flexible rubber and enclosed in a plexiglass frame. (b) Schematic side-view section of DULAB showing (from bottom to top) the car jacks' differential uplift configuration used in the experiment reported here, the step-like topography of the prisms, the stretching rubber, rigid plates, and the measured topography of the surface (red profile). The topographic profile was measured following a calibration stage

conducted without precipitation and erosion by surface runoff. The spatial uplift gradient shown in (a) does not reflect the gradient used in the experiment and simulations. Rigid plates are not shown in (a) to highlight the behavior of the rubber.

2.1.2 Experimental protocol

We explored a double-stage tectonic scenario. First, we imposed uniform uplift (Figure 2a) until a topological quasi steady state was achieved, whereby the drainage network topology experienced only minor changes (Hasbargen & Paola, 2000; Reinhardt et al., 2015; Goren et al., 2014). Second, we imposed a differential uplift in the form of tilting, as shown in Figure 2b. Notably, the prisms' geometry allows tilting across 2/3 of the domain width, with uniform uplift across the remaining 1/3, as shown in Figure 1b.

In preparation for the experiment, the plexiglass frame was filled with the experimental material, which was left to settle for approximately 24 hours, allowing the material to compact by a few millimeters, and release excess water and air. The experiment began when we simultaneously applied uplift and precipitation. The average precipitation rate we induced was $65\ \frac{mm}{hour}$ with a standard deviation to average ratio of 15%.

To document the evolving experimental landscape, precipitation was paused every 30 minutes for a duration of three minutes. During this pause, 17 photographs were taken from different locations and angles using a Nikon B500 (16MP) digital camera. Each set of 17 photographs was used to generate a 3D model of the landscape and a 0.5 mm/pixel Digital Elevation Model (DEM) using the commercial "Agisoft Metashape Professional" software. With this approach, we analyzed the evolution of the experimental landscape based on a time series of DEMs.

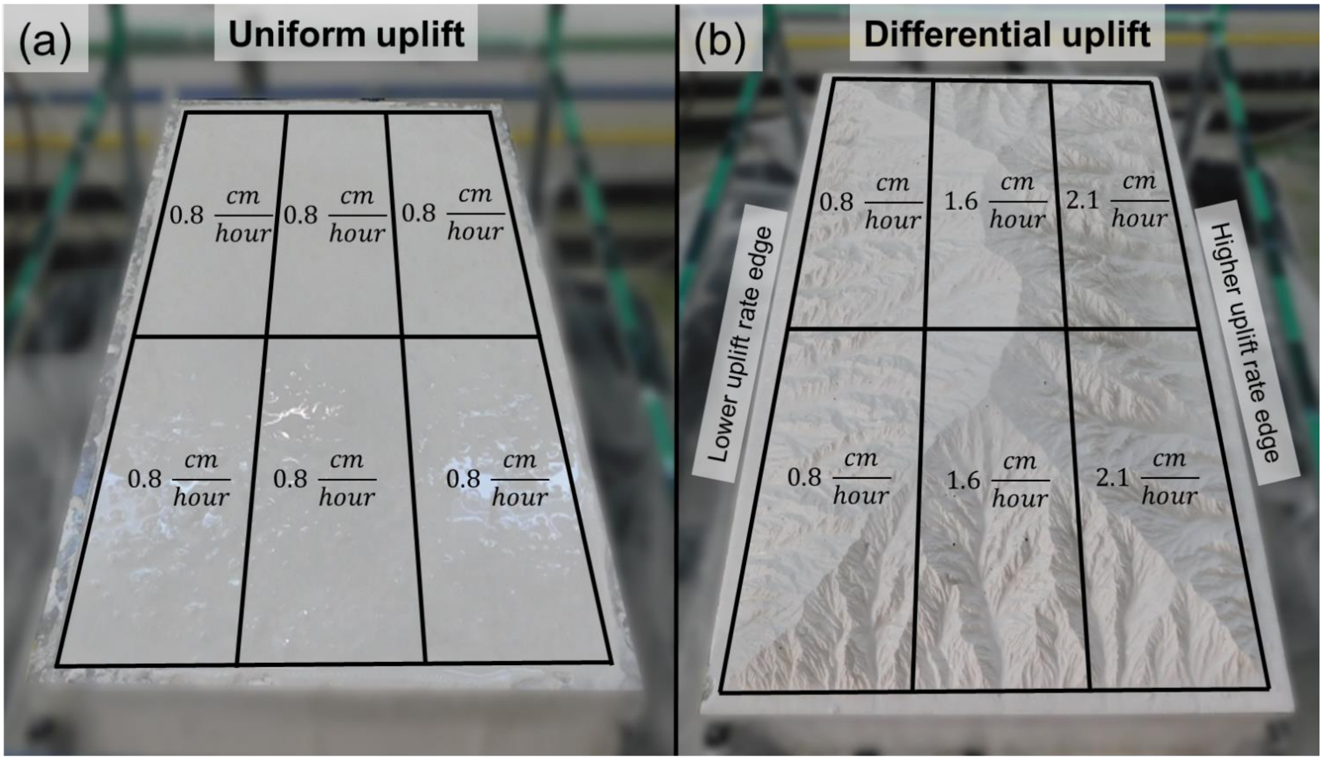

Figure 2: Perspective-view photos of DULAB's plexiglass frame filled with the experimental material and schematics of the spatial trend of uplift set by the uplift rate of the six jacks. (a) Initial conditions of zero topography for the first stage of uniform uplift. In this stage, all six car jacks uplifted at the same rate. (b) Initial conditions for the second, differential uplift, tilting stage that began with a developed topography and a stable main water divide at the center of the domain. In this stage, the car jacks were uplifted in pairs, resulting in three uplift bands.

2.2 DAC – Divide and Capture

2.2.1 Model setup

The landscape evolution model, DAC (Goren et al., 2014), combines a numerical solver for fluvial incision over a triangular, irregular, and sparse grid, with analytical solutions for the fluvial and hillslope topography at the sub-grid scale. The numerical solver implements the stream power incision model (e.g., Howard et al., 1994; Whipple & Tucker, 1999):

(1) $E = K(PA)^m S^n$

Where E [$\frac{L}{T}$] is erosion rate, K [$\frac{L^{1-3m}}{T^{1-m}}$] is erodibility coefficient, P [$\frac{L}{T}$] is precipitation rate, A [L^2] is drainage area, S [$\frac{L}{L}$] is channel gradient, and m and n are positive exponents. Hillslope topography is modeled as a steady-state diffusion profile with respect to the incision rate of the proximal channel node. A cutoff threshold slope truncates the diffusive profile. With this approach, DAC locates the position and elevation of all water divides through time, identifies capture events based on a divide breaching algorithm, and resolves continuous sub-grid changes in basin geometry and drainage area. In the current study, DAC simulations were performed on a rectangular domain with four equal-elevation base levels (e.g., Goren et al., 2014; Willett et al., 2014). Like the DULAB experiment (Section 2.1), we utilized DAC to examine a double-stage tectonic scenario. We applied constant and uniform uplift and precipitation rates on a subdued random topography until the mean and maximum topographic relief stabilized and topological quasi steady state was achieved (Hasbargen & Paola, 2000; Reinhardt et al., 2015; Goren et al., 2014). Then, we applied tectonic tilting, in a pattern similar to the rubber geometry in Figure 1b, in which the uplift rate is given by $U(\tilde{x}) = U_1 + \lambda\tilde{x}$, for $0 < \tilde{x} < \frac{2M}{3}$ and $U = U_1 + \lambda(\frac{2M}{3})$ for $\frac{2M}{3} \leq \tilde{x} < M$, where U_1 is the uplift rate ($\frac{L}{T}$) on the lower uplift rate edge, λ is the linear uplift rate gradient ($\frac{L}{T}$ per L), M is the width of the domain, and $\tilde{x}$ is the distance measured from the lower uplift rate edge (see Table 1 for simulation parameters). Tilting was applied until a new quasi steady state was achieved. In order to apply the same morphometric analysis over DAC numerical surfaces as done over DULAB experimental surfaces, we interpolated DAC's topography from its original triangular grid into a structured grid (DEM) with a spatial resolution of 20 m/pixel.

2.2.2 DAC simulation parameters

We performed two DAC simulations that differ in their model parameters. The first simulation was designed to facilitate comparison between numerical and experimental landscapes. Comparison was achieved by ensuring that the scale factors for converting between the experiment and simulation parameters and outcomes were internally consistent. The channel profile in the experimental landscape was measured to have a relatively low concavity, ($\theta = \frac{m}{n} \sim 0.15$), typical of experimental landscapes produced with similar experimental material (e.g., Crave et al., 2000; Lague et al., 2003; Bonnet & Crave, 2006). This concavity was implemented in the first DAC simulation by using n = 1.8 and m = 0.28. In relation to the length scale, the experimental maximum relief at the end of the uniform uplift stage was approximately 6 cm. Given that DAC domain width ($M_{simulation}$) was chosen to be 50 km (defining an experiment-to-simulation length scale factor of $L_0 = \frac{M_{experiment}}{M_{simulation}} = 10^{-5}$), the target numerical maximum relief at the end of the uniform uplift stage was 6 km in this simulation. To achieve this target relief, we estimated the fluvial relief at the channel head, $z(x_c)$ using a 1D approximation (Willett, 2010):

$$(2)\ z(x_c) = \left(\frac{U}{KP^m {k_a}^m}\right)^{\frac{1}{n}} \frac{1}{1-\frac{Hm}{n}} \left(\left(\frac{M}{2}\right)^{1-\frac{Hm}{n}} - {x_c}^{1-\frac{Hm}{n}}\right)$$

Where U is uplift rate, k_a is inverse Hack's scaling coefficient, H is inverse Hack's exponent (Hack, 1957), and x_c is hillslope length. Equation 2 constrains the relation between the parameters U, K and P that would satisfy the target elevation given m and n. We therefore chose U, K, and P such that the vertical velocity scale factor (defined by the ratio of the experiment-to-simulation uplift rate) was consistent with the horizontal velocity scale factor (defined by the experiment-to-simulation ratio of basins elongation rate, V_h ; see section 0). We found that defining a velocity scale factor of $U_0 = 8.76 * 10^4$, such that 1 cm/hour in the experiment corresponds to 1 km/Myr in the simulation was consistent for both applied vertical uplift rate ratio and the emerged horizontal basin growth rate ratio.

Consequently, the time scale factor is $T_0 = \frac{L_0}{U_0} = 1.14 * 10^{-10}$, indicating that a duration of one hour in the experiment is approximately equivalent to 1 Myr of DAC simulation. This simulation is referred to as “low concavity”.

Since the concavities measured in the experiment and incorporated in the low concavity simulation are lower than those measured in most natural landscapes (e.g., Tucker & Whipple, 2002), we performed an additional simulation with a higher concavity ($\theta = 0.45$). In this simulation, the erodibility coefficient was chosen such that the quasi steady state relief with the same uniform uplift rate as in the low concavity simulation was approximately 3 km, to better simulate the relief of a natural terrain.

Both simulations were performed in a 200 x 50 km^2 domain. The high concavity simulation was repeated also in a shorter domain (90 x 50 km^2), with scaled dimensions similar to the DULAB domain, and a longer domain (1000 x 50 km^2) in order to increase the number of basins in the emerging landscape, improve statistical inferences, and ensure observations of rare basin dynamics. The full list of parameters for the simulations and experiment is shown in Table 1.

Table 1: Parameters used in the experiment and simulations. Additional model parameters used in the DAC simulations are the same as Goren et al. 2014; Table 1.

Input parameters	**Experiment**	**Low concavity simulation**	**High concavity simulation**
***L x M* (Domain size)**	90 x 50 cm^2	200 x 50 km^2	90 x 50 km^2 200 x 50 km^2 1000 x 50 km^2

U_1 **(Uniform uplift rate)**	$0.8\ \frac{cm}{hour}$	$0.8\ \frac{km}{Myr}$	$0.8\ \frac{km}{Myr}$
$U(\tilde{x})$ **(Differential uplift rate)**	$0.8-1.6\ -$ $2.1\frac{cm}{hour}$	$0.8-1.6\ -2.1\frac{km}{Myr}$	$0.8-1.6\ -2.1\frac{km}{Myr}$
λ **(Uplift gradient)**	$0.039\ \frac{cm}{hour}$ per km	$0.039\ \frac{km}{Myr}$ per km	$0.039\ \frac{km}{Myr}$ per km
P **(Precipitation rate)**	$65\frac{mm}{hour}$ $\pm 10\%\ to\ 15\%$	$1\frac{m}{yr}$	$1\frac{m}{yr}$
K **Erodibility**	-	$1.48 * 10^{-4}\ [m^{0.16}yr^{-0.72}]$	$10^{-5}\ [m^{-0.35}yr^{-0.55}]$
m **Discharge exponent**	-	0.28	0.45
n **Slope exponent**	-	1.8	1
x_c[a] **Critical**	?[b]	$0.7\ [km]$	$0.7\ [km]$

hillslope length			
$\boldsymbol{H}$ [a] **Inverse Hack's exponent**	-	1.67	1.67
$\boldsymbol{k_a(H)}$ [a] **Inverse Hack's coefficient**	-	0.73 $[km^{2-H}]$	0.73 $[km^{2-H}]$

[a]Parameters that affect the analytical sub-grid solver in DAC (Goren et al., 2014).

[b]In the experiment, channelization reached very close to the divide (Sweeny et al., 2015; Turowski et al., 2006), hence x_c is negligible.

2.3. Geomorphic Analysis

Using the DEMs generated for the experiments and simulations, we applied standard flow routing procedures using ArcGIS to identify and extract the boundaries of drainage basins. The drainage network was defined based on a threshold drainage area of 2.5 cm^2 in the experiment and 0.5 km^2 in the simulations. Note that this threshold area was chosen for convenience, and it does not reflect initiation of channelization. During the uniform uplift rate stage, the drainage network evolved by incising into a transient, uplifting plateau. The plateau boundaries were manually delineated and removed from this analysis. Delineation was based on a combination of slope and aspect rasters.

Drainage basins were categorized based on their association with the main divide or plateau edges and based on their outlet location (Figure 3). Basins with boundaries that reached the main water divide or the boundaries of the uplifting plateau and drained to the long edges of the domain are referred to as "main basins". Basins that are positioned between main basins are referred to here as "nested basins" (Shelef, 2018) ("interstitial basins," Walcott & Summerfield, 2009). Other basins were not analyzed in this work. To quantify the evolution of basins' geometrical scaling relations, we calculated time series of Hack's coefficient and exponent (Dodds & Rothman, 2000; Mueller, 1973; Sassolas-Serrayet et al., 2018; Cheraghi et al., 2018; Bennet et al., 2016) and the spacing ratio, R, (Hovius, 1996; Talling et al., 1997) for basins in the experimental and numerical landscapes.

Hack's parameters were extracted based on a nonlinear, power-law regression through the data of the drainage area and mainstream length along confluence pixels. To define an error on the measured Hack's parameters, we performed 5000 bootstrapping iterations, where in each iteration, Hack's parameters were computed based on randomly sampled 50% of the L and A data. We report the mean and standard deviation of the sampled populations. This analysis was performed on main and nested basins, based on their position at the time of main divide formation. The spacing ratio, however, was calculated only for main basins as $R = \frac{\bar{D}}{\bar{S}}$, where $\bar{D}$ was computed by averaging main basins' maximal diameter, measured as the length of the long axis of the minimum-bounding convex polygon (based on ArcGIS Minimum Bounding Geometry tool), and $\bar{S}$ measured as the average outlet spacing, namely, the average distance between a basin's outlet and the outlets of its neighboring main basins (Figure 3). In section 3.1, geometrical scaling relations in the higher and lower uplift rate sides are depicted with different symbols.

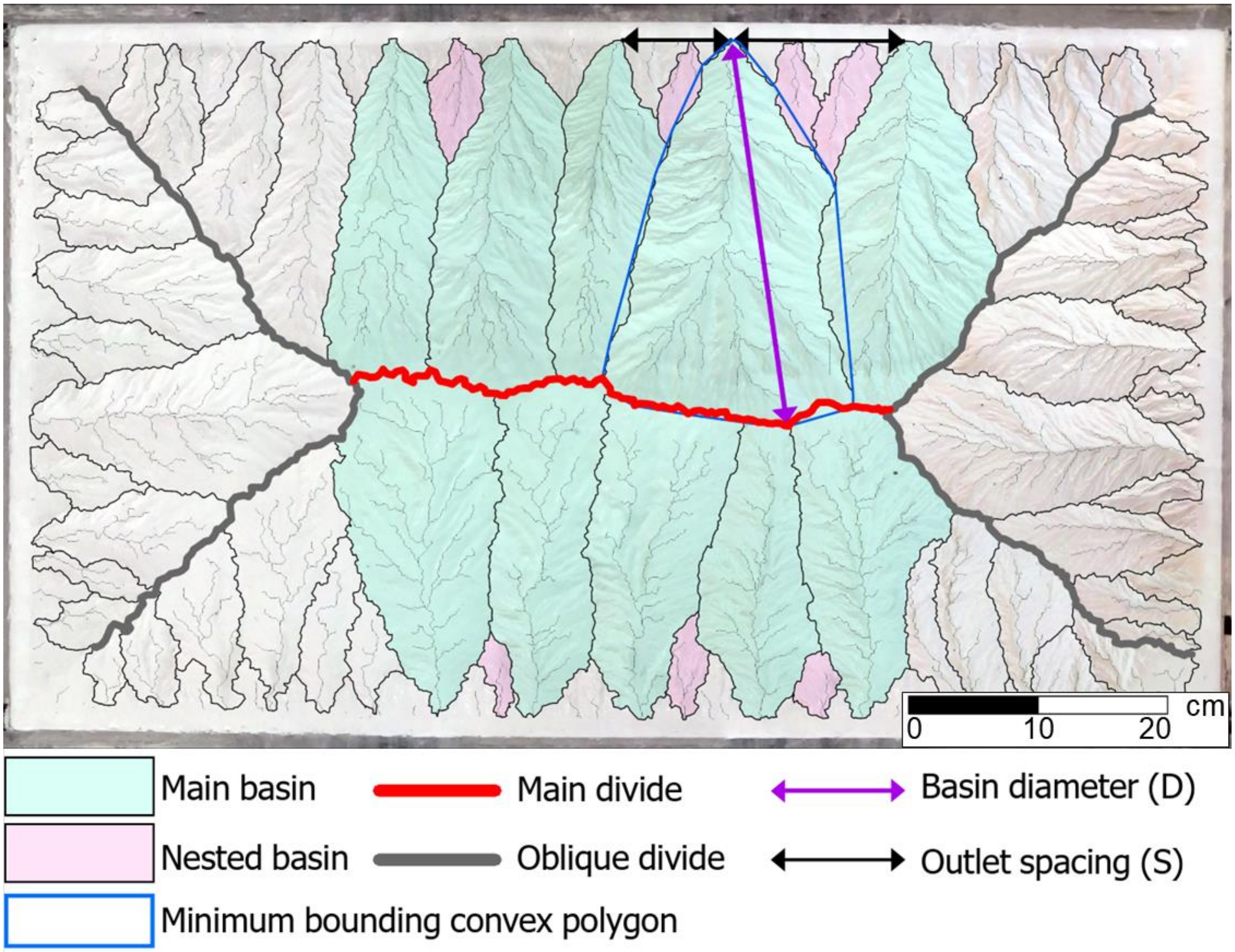

Figure 3: Orthophoto of DULAB landscape at the end of the uniform uplift rate stage, showing the main geometric features refered to in the experimental and numerical landscapes analysis. Shaded green and pink areas show main and nested basins, respectively. Only nested basins that were successfully delineated across sequential time-steps are shown in this figure. Grey and red lines mark the oblique and main water divides, respectively. Purple arrow marks basin diameter, D, measured as the long axis of the minimum bounding convex polygon (blue). Black arrow marks basin spacing, S.

2.3.2. Main divide geometry and evolution

The drainage divide network was extracted using TopoToolBox (Schwanghart & Scherler, 2014). To focus on the main drainage divide, the divide network was truncated based on a threshold distance to a divide endpoint calculated over a tree-like sorted divide network (Scherler & Schwanghart, 2020a). The threshold distance was 55 km in the numerical landscapes, and it ranged between 60 cm – 70 cm in the experimental landscape. 'Main divide asymmetry' (Bonnet, 2009; He et al., 2021; Shi et al., 2021) is defined as the ratio of main divide average position relative to the lower uplift rate edge ($\tilde{x} = 0$) to the domain width (M). Time series of main divide asymmetry allows the estimation of the main divide's migration rate.

2.3.3. Main divide stability and drainage reorganization

Two metrics were used to map divide stability and explore the consistency of this mapping with the observed trends of divide migration and network reorganization (e.g., Guerit et al., 2018). The first metric, χ-analysis (Willett et al., 2014), accounts for the topology of the whole drainage network and is therefore considered a measure of long-term stability (Forte et al., 2018). Under steady-state conditions, when erosion rate, *E*, and tectonic uplift rate, *U*, are balanced ($\frac{\partial z}{\partial t} = 0$), the stream power incision model, Equation (1) predicts:

(3) $S = \frac{dz}{dx} = (\frac{U}{KP^m})^{\frac{1}{n}} A^{-\frac{m}{n}}$

Equation (3) can be integrated to yield (e.g., Perron & Royden, 2013):

(4) $z(x) = z_b + (\frac{U}{KP^m A_0^m})^{\frac{1}{n}} \chi,$

with:

(5) $\chi = \int_{x_b}^{x} (\frac{A_0}{A(x)})^{\frac{m}{n}} dx,$

where z_b is the channel elevation at the base level, and A_0 is a reference drainage area that sets χ units to length. Based on Equation (4), the parameter χ is used as a proxy for the steady-state elevation of river channels (Willett et al., 2014; Perron & Royden, 2013). Differences in the χ value of opposite equal-elevation channel heads, could indicate that the drainage topology is not stable. Namely, the relationship between slope and drainage area do not obey Equation (3). Hence, to regain topological stability and bring the system toward equilibrium, a divide is expected to migrate toward the basin with the higher χ channel head (Willett et al., 2014). When uplift rate is uniform, χ takes the form presented in Equation (5). Otherwise, in the case where U is non-uniform, a different steady-state elevation proxy (χ') can be obtained by incorporating the known spatial uplift gradient (Willett et al., 2014):

(6) $\chi' = \int_{x_b}^{x} (\frac{U(x){A_0}^m}{A(x)^m})^{\frac{1}{n}} dx$

Analysis based on χ and χ' was performed over both numerical and experimental landscapes.

The second metric is the relief gradient across divide that characterizes a shorter time scale stability (Forte et al., 2018), and is applied only to the main divide. This metric calculates the local relief (*LR*) adjacent to the divide, quantified as the elevation difference between a pixel on the main divide and the nearest pixel whose drainage area is equal to the threshold drainage area used to define the drainage network. Divide stability is quantified as the across-divide difference in local relief normalized by the sum of across divide relief, also referred to as Divide Asymmetry Index (after Scherler & Schwanghart, 2020a, 2020b): $DAI = \left|\frac{\Delta LR}{\sum LR}\right|$. This index is computed for main divide segments in both stages of the experiment and simulations from the point a main divide is fully established.

3. Results

3.1. Plan-view landscape evolution

In this section we describe changes in quantity, area, the associated divide migration and the observed modes of reorganization during the double-stage tectonic scenario.

At the beginning of the experiment and simulations, drainage basins emerged at the periphery of the rectangular domain and grew toward the center by incising an uplifting plateau. As basins grew in size, they elongated and widened until channels completely dissected the landscape and a system of drainage divides formed, consisting of a long edge-parallel main divide and four oblique divides (Figure 3). During this stage, the number of main basins gradually decreased as a subset of basins gained drainage area, while others stopped growing or shrank.

Several fluvial reorganization processes were observed to contribute to this differential growth effect (for detailed statistics see table S1 ,Supplementary material). We categorize these processes into (1) beheading via stream capture that preserves the drainage pattern of the captured area, and (2) gradual beheading, in which gradual divide migration at the headwaters erases the drainage pattern of the shrinking basin. In some cases, these modes induce triple divide junction migration (Figure 5). χ analysis of the numerical landscapes revealed across divide χ gradients prior to documented reorganization events, consistent with the orientation of the observed divide migration (Figure 5a, c). In the experiment, across divide χ gradients were mostly consistent with the occurrence and sense of drainage reorganization (Figure 5b,d), and the few cases where χ gradients were not consistent appear to be related to topographic and topological changes that occurred in between time steps (Guerit et al., 2018). These reorganization processes persisted until the main drainage divide formed and quasi steady state was achieved.

Similar to previous studies (Hasbargen & Paola, 2000, 2003; Bonnet & Crave, 2003, 2006; Lague et al., 2003; Goren et al., 2014, Willett et al., 2014; Reinhardt et al., 2015), we observed that even after the main divide formed, ongoing reorganization continued, with minor changes to basins boundaries.

At the second stage of the experiment and simulations, as the tectonic conditions changed from uniform uplift to tilting, the landscape responded by main divide migration towards the higher uplift rate side, consistent with theory, previous simulations, and field observations (Goren et al., 2014; Willett et al., 2014; Forte et al., 2015; He et al., 2019, 2021; Shi et al., 2021; Shikakura et al., 2012). As a consequence, basins that drained to the higher uplift rate edge (Figure 2b) underwent continuous area reduction as the migrating main divide gradually beheaded their headwaters. Basins draining to the lower uplift rate edge increased their size by elongating, overall generating an asymmetric topography. In particular, main divide segments migrated a distance of 2 to 5 cm in the experiment, 2 to 4 km in the low concavity simulation, and 1 to 7 km in the high concavity simulation. Figure 6 shows the evolution of the main divide asymmetry in the experiment and simulations (200 x 50 km^2).

Upon the application of tilting and during the onset of main divide migration, χ' gradients across the main divide were measured to be high (Figure 7c) and thus predict migration toward the higher uplift rate side, while DAI values were measured to be low (Figure 8c) and thus their predicted migration directions are variable. By the end of this stage χ' gradients have decreased significantly (Figure 7d), meaning that the landscapes reached a stable configuration with respect to the applied uplift rate gradient (Willett et al., 2014). Despite that, DAI values have increased and consistently point toward the higher uplift rate side (Figure 8d).

In addition to main basins' area change during main divide migration, the number of main basins changed as well. Results from the high concavity simulation (1000 x 50 km^2) reveal that along the higher uplift rate side, the number of main basins increased as the migrating main divide intersected the waterheads of nested basins that did not reach it before the application of tilting (Figure 9), merging their triple divide junction with the main divide. An opposite behavior was observed on the lower uplift rate side, where relatively narrow main basins were disconnected from the main divide and became nested basins. This occurred in parallel to elongation and widening of their neighboring main basins that kept pace with the migrating divide, generating new triple divide junctions. In some cases, the disconnected basins maintained a stable size, but in others, they were beheaded by both gradual divide migration and abrupt stream captures, causing the recently generated triple divide junction to migrate toward the outlet of the basins. Furthermore, we observed that the channel heads of the narrow, disconnected basins in this simulation were characterized by higher χ values relative to their neighboring main basins before the tilting stage (Figure 9, inset). Overall, in this simulation four new basins were incorporated to the main divide on the higher uplift rate side following the tilting, increasing the number of main basins on this side by 5%. On the lower uplift rate side, ten basins were disconnected from the main divide, decreasing the number of main basins on this side by 12%.

In the experiment, where the domain length to width ratio was relatively small (90 x 50 cm^2), as well as the number of main basins, we observed that upon divide migration, a single main basin was incorporated to the main divide along the higher uplift rate side, increasing the number of main basins on this side by 20% (from 5 to 6). We did not observe disconnected basins on the lower uplift rate side in the experiment and the low concavity simulation, and the number of main basins remained constant on this side. Similar behavior was observed in the 90 x 50 km^2 high concavity simulation.

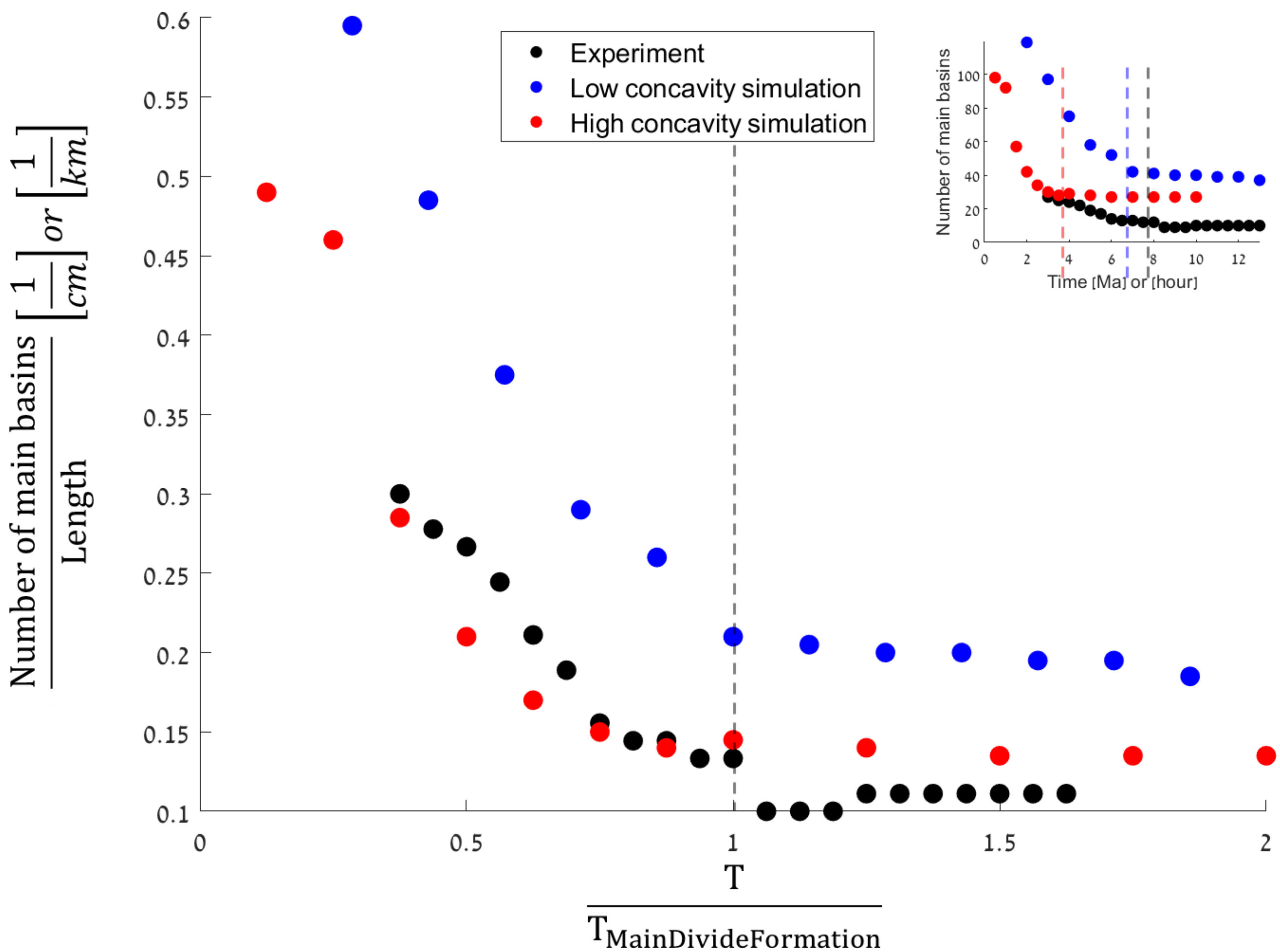

Figure 4: Number of main basins normalized to the length of the long edge of the domain as a function of time normalized to the timing of main divide formation in DULAB experiment and DAC simulations. Vertical dashed line indicates the timing of main divide formation ($T / T_{MainDivideFormation} = 1$). Simulation results presented here were conducted on a 200x50 km^2 domain. Inset shows the number of main basins as a function of time in the experiment (in hours) and the simulations (in Myr) with colored vertical dashed lines indicating the relevant timing of main divide formation.

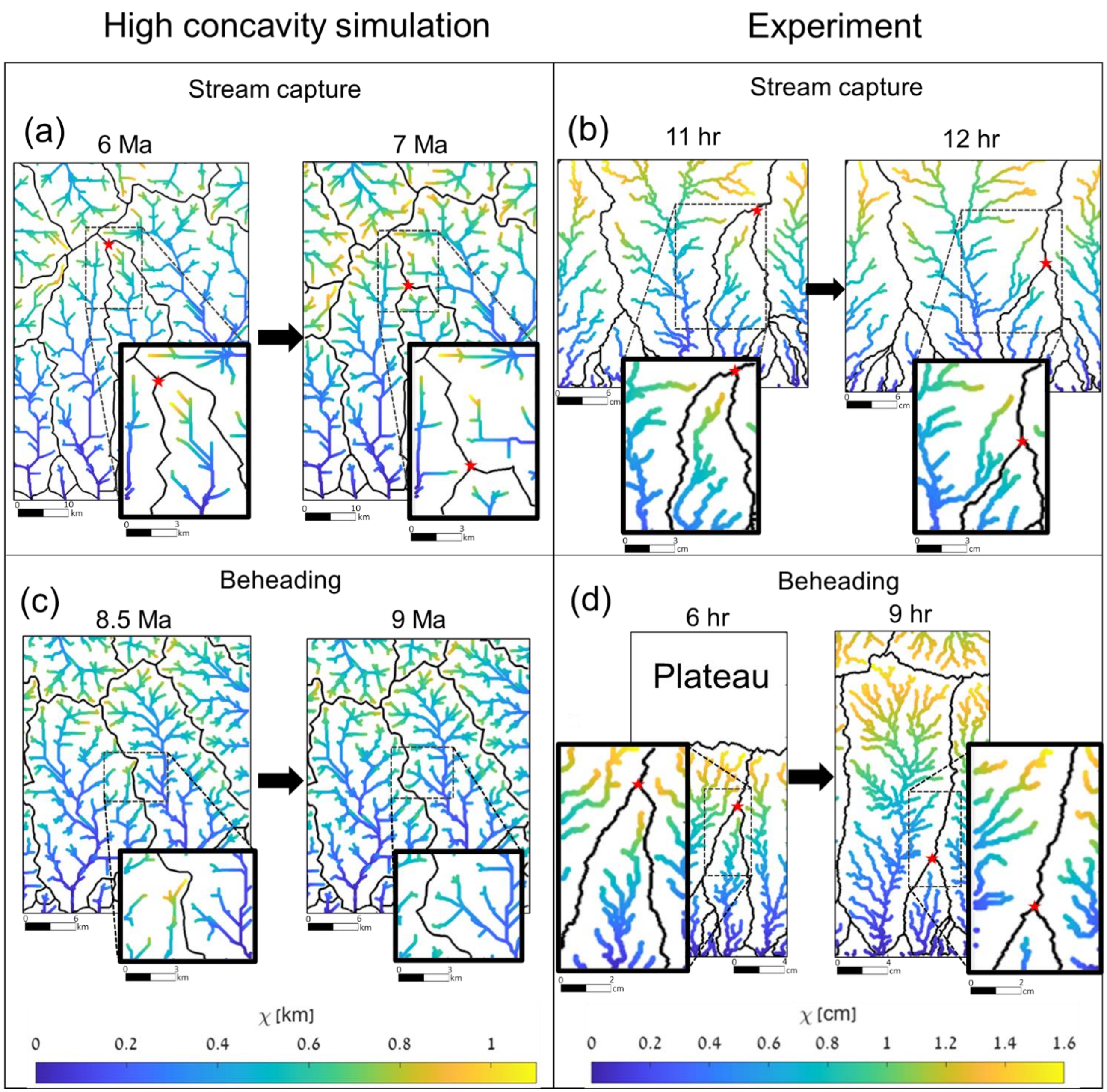

Figure 5: Modes of reorganization observed in the high concavity simulation (1000x50 km^2) (a and c) and in the experiment (b and d) during the uniform uplift stage. (a) and (b) show examples of beheading by stream capture and (c) and (d) show examples of gradual beheading. Both processes may induce triple divide junction migration toward the outlet of the nested basin (a, b, d) or lateral divide shift between two basins (c). The insets focus on the area of interest. The drainage network is color-coded by

χ values, and the color bar is rescaled to highlight across-divide χ differences in the insets. χ differences across divide before the migration are consistent with the direction of divide motion. Red stars mark triple divide junctions. In the calculation of χ a reference drainage area of $A_0 = 10^{-2}$ km^2 in the simulation and $A_0 = 10^{-6}$ cm^2, in the experiment were used.

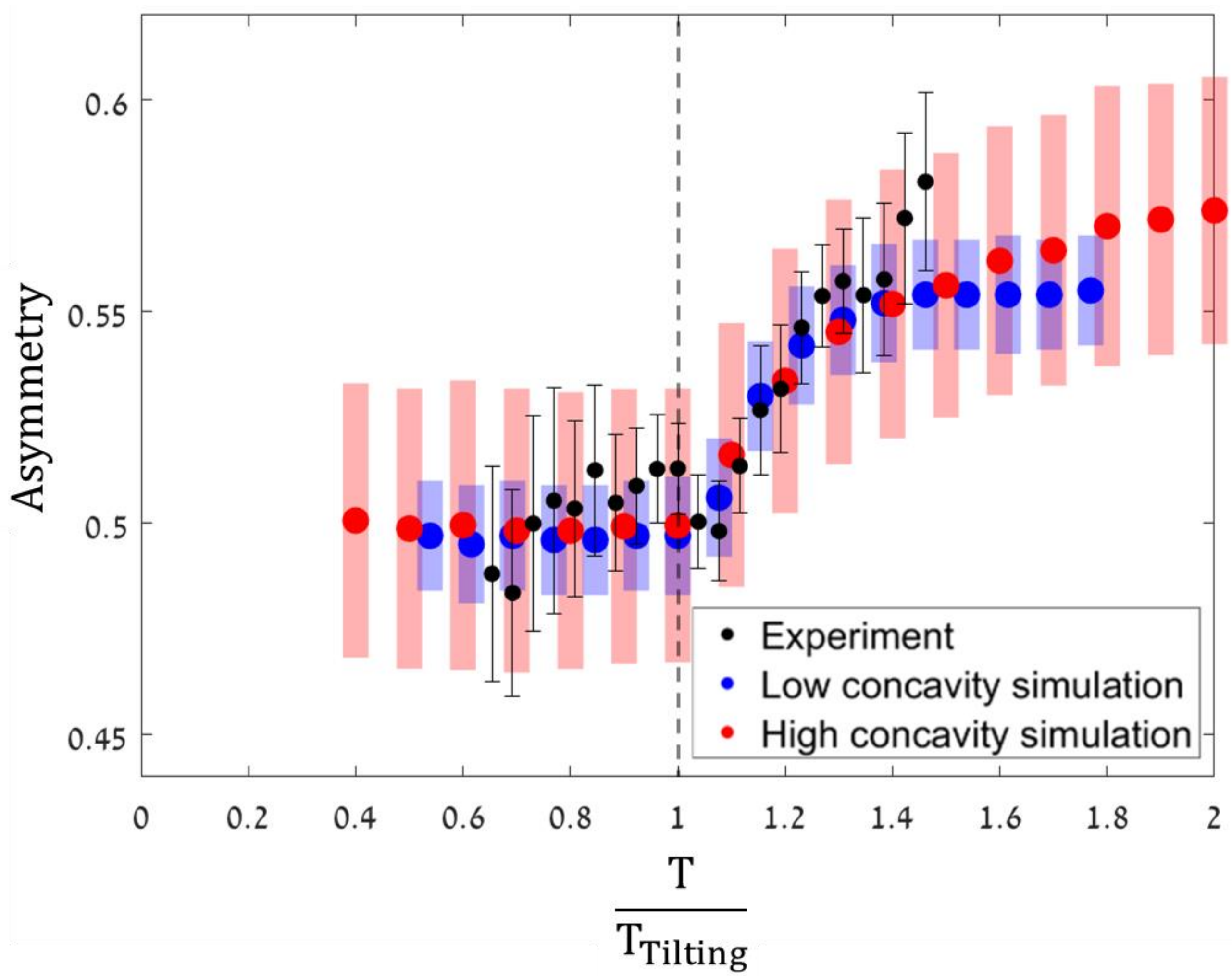

Figure 6: Main divide asymmetry computed using the average divide position relative to the domain width in the experiment and simulations (200x50 km^2). This figure shows the temporal change in asymmetry before (for reference) and during tilting. The vertical dashed line at $T/T_{Tilting} = 1$ marks the

onset of tilting). Error bars and colored bars represent standard deviation of the average location of segments of the main divide in the experiment and simulations, respectively.

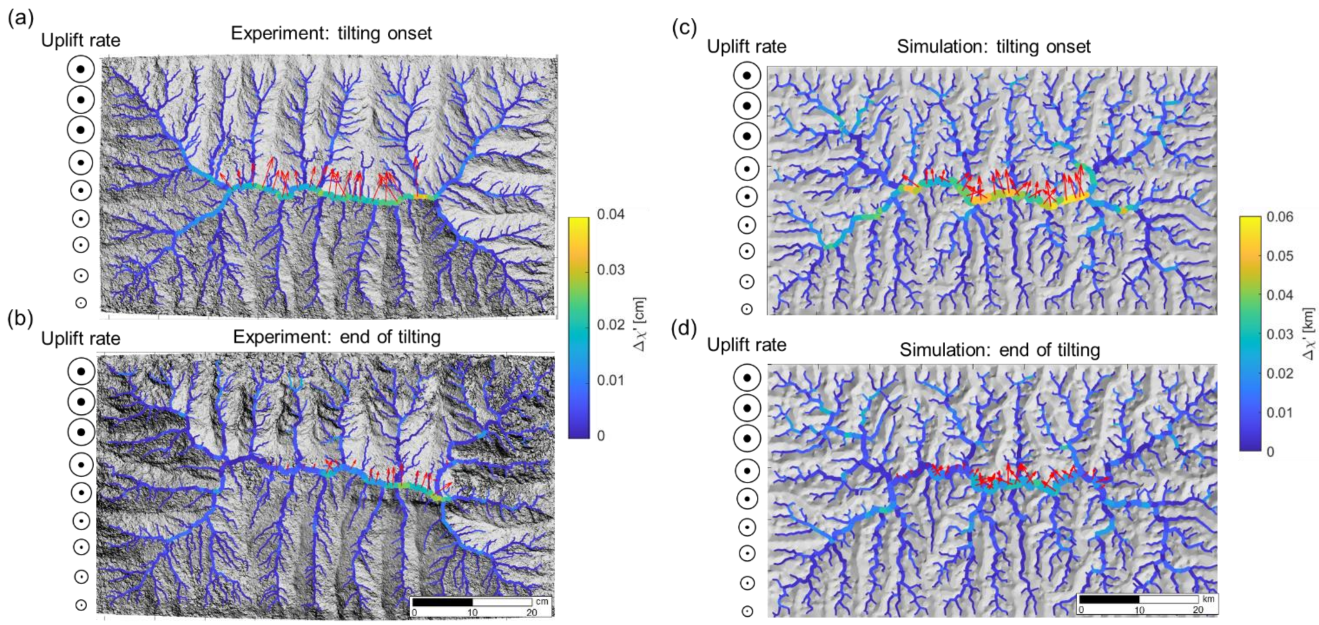

Figure 7: Hill-shade maps showing the drainage divide network colored by the cross-divide difference in χ' before and after the tilting stage in the experiment (a, b), and the high concavity simulation (90 x 50 km^2) (c, d). Red arrows along the main divide point toward the direction of higher χ' values, which is also the theoretically expected direction of divide migration toward the higher uplift rate side (Goren et al., 2014; Willett et al., 2014; Forte et al., 2015), as depicted by the side black arrow heads. Red arrows lengths reflect the magnitude of χ' gradient. This analysis is based on Scherler and Schwanghart (2020a, 2020b) and was executed in TopoToolBox with A_0 = 2 cm^2 or 2 km^2. χ' is calculated based on eq. (6) with the applied U(x). Note how χ' gradients across the main divide decrease from the onset of tilting application (a and c) to the end of the simulation and experiment (b and d). This difference indicates that with main divide migration, the landscape achieves a topologically more stable configuration with respect to the applied uplift rate gradient.

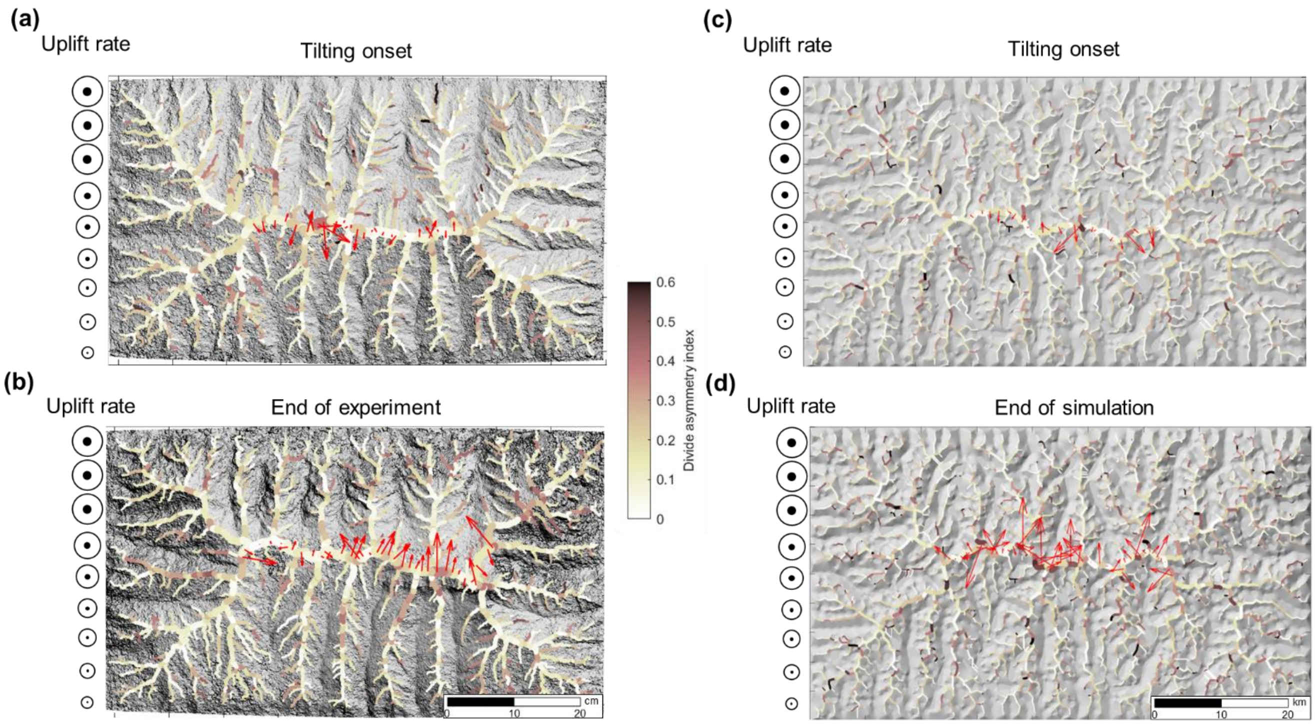

Figure 8: Hill-shade map showing the drainage divide network colored by DAI ("Divide Asymmetry Index", Scherler and Schwanghart (2020a, 2020b)) before and after the tilting stage in the experiment (a, b), and the high concavity simulation (90x50 km^2) (c, d). Red arrows point toward the direction of the lower local relief. Arrows lengths reflect the magnitude of the DAI. Upon the application of tilting and during the onset of divide migration (a and c) the magnitude of the DAI is small, and its predicted orientation is variable. At the end of the experiment and simulation, after the landscapes have achieved a more stable configuration and the main divide is relatively stationary (b and d), the magnitude of the DAI is high, and it consistently points in the direction of the higher uplift rate side

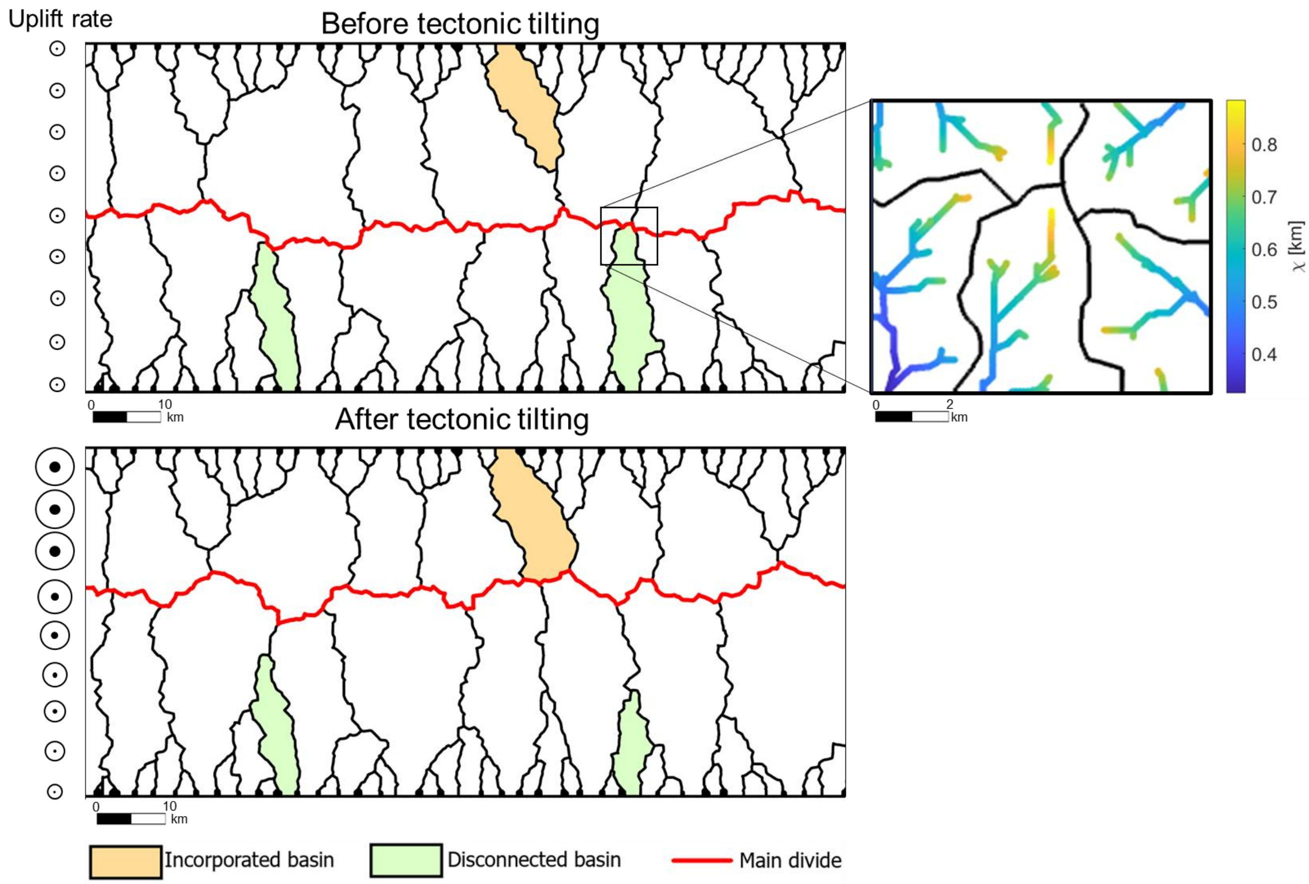

Figure 9: Sections from a high concavity simulation (1000 x 50 km^2) showing drainage basins incorporated (orange) and disconnected (green) from the main divide as an outcome of main divide migration in response to tilting. The red line depicts the main drainage divide. The inset focuses on a disconnected basin's headwaters and shows the χ map of the drainage network in the surrounding basins'. Before disconnection, the disconnected main basins' headwaters are characterized by relatively high χ values.

3.2. Geometrical scaling relations during landscape change

3.2.1. Spacing ratio

Changes in basin spacing ratio reflect the evolution of basin diameter and changes in outlet spacing. Figure 10a shows that in both the experiment and the 200 x 50 km^2 simulations, main basins exhibited a linear trend of basin elongation (diameter increase) with time during the plateau incision stage and until the main divide was formed, indicating a constant and uniform rate of plateau shrinkage. The rate of inward plateau shrinkage, corresponding to the rate of main basin elongation (Figure 10a) was observed to be fastest in the high concavity simulation ($V_h = 7.72\ \frac{km}{Myr}$) compared to the low concavity simulation ($V_h = 3.59\ \frac{km}{Myr}$) and to the experiment ($V_h = 3.51\ \frac{cm}{hour}$, which corresponds to 3.51 $\frac{km}{Myr}$ when using the time scale factor, T_0).

Similar to basins' diameter increase, we observed that during the same stage, before the main divide formed, basins' average spacing (S) also increased linearly (Figure 10b), assisted by fewer basins that reached the plateau and drained it through time. Once the main divide formed, D and S remained relatively constant. The relative rates of D and S increase during the plateau incision stage, initially led to an increase in the spacing ratio, R by up to 50% in the experiment and low concavity simulation and by up to 30% high concavity simulation. Eventually, R stabilized with a mean value between 2.1 to 3.3 at the end of the uniform uplift stage (Figure 10c). We emphasize that from the earliest stages of basins' evolution, despite the increase of experimental and numerical R values, it remained within the reported range for natural uplifted blocks and linear mountain ranges (Hovius, 1996; Talling et al., 1997; Walcott & Summerfield, 2009).

After the application of tilting, we observed that R remained within the same narrow range, despite main divide migration that led to basin elongation (D increase) on the lower uplift rate side and basin shortening (D decrease) on the higher uplift rate side (Figure 10, $T/T_{Tilt}>1$). The incorporation of nested basins to the main divide on the higher uplift rate side, acting to decrease S, and the disconnection of main basins from the main divide on the lower uplift rate side, acting to increase S, assisted in maintaining approximately constant R values on both sides of the main divide in the high concavity simulation (1000 x 50 km^2). Importantly, in the experiment and in the 200 x 50 km^2 simulations, we did not observe this effect on the lower uplift rate side as the divide migrated, hence R slightly increased due to basins elongation. Despite that, R remained within the same narrow range of values.

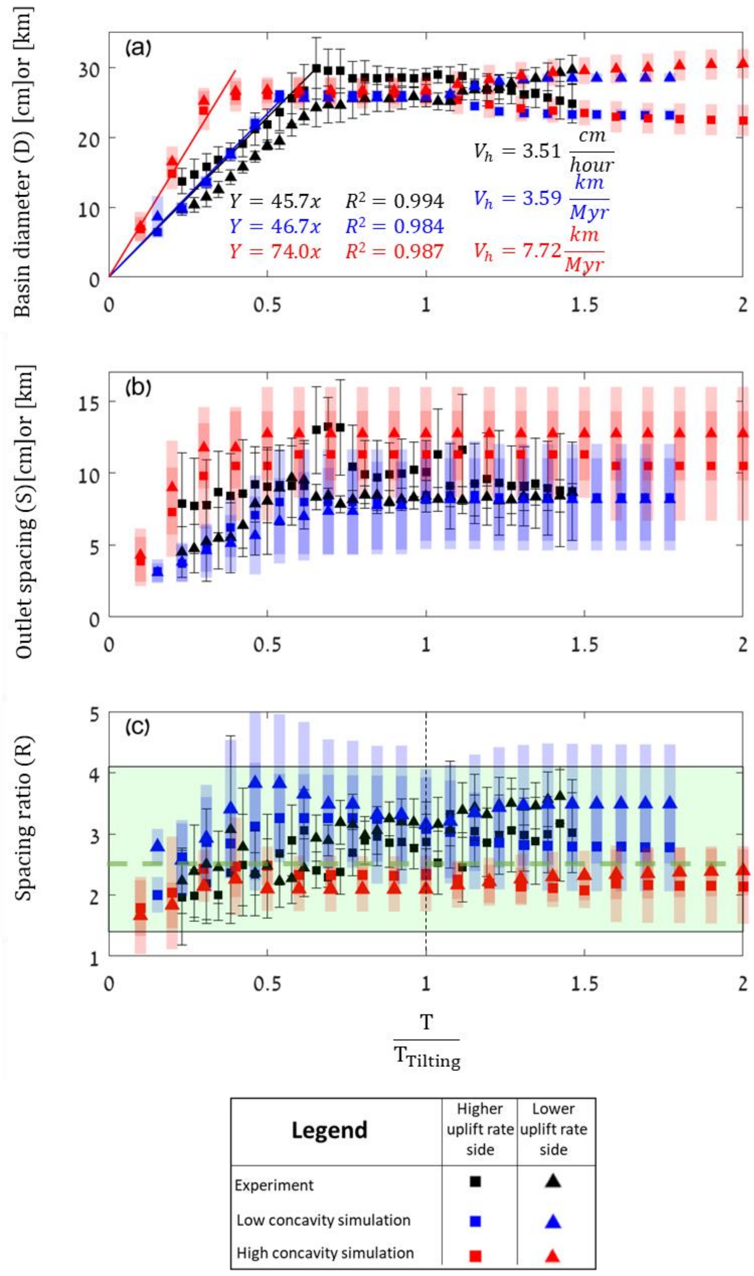

Figure 10: Temporal evolution of main basins' geometrical parameters on the higher (squares) and lower (triangles) uplift rate sides of the landscapes during uniform ($T/T_{Tilting}<1$) and differential

($T/T_{Tilting}$>1) uplift in the experiment (black) and simulations (blue and red). Panels show the evolution of (a) basin diameter (D), (b) outlet spacing (S), and (c) spacing ratio (R), the ratio between D and S. Green rectangle and dashed line in (c) show the range of values and average of naturally observed R values in fault-bounded blocks, respectively, as reported by Talling et al. (1997). Linear regression lines and equations in (a) refer to data from the onset of the experiment/simulation until the main divide formed. In all panels, error bars and colored bars represent the corresponding geometric parameter's standard deviation.

3.2.2. Hack's parameters

During the uniform uplift stage, the Hack's exponent of the numerical main basins (200 x 50 km^2) initially decreased steadily and then increased before reaching a stable value approximately at the time of main divide formation (Figure 11a). An opposite trend was observed for the evolution of Hack's coefficient (Figure 11b). The temporal signal of Hack's parameters in the experimental main basins was too noisy to detect a similar trend. During the tilting stage, numerical main basins showed no significant change in Hack's exponent (Figure 11a), despite the drainage area change inflicted by the migrating divide. Only a small decrease was observed in the Hack's coefficient of the basins on the higher uplift rate side (Figure 11b). Throughout most of their evolution, main basins' Hack's parameters remained within the natural range of values reported in previous studies (e.g., Hack, 1957; Montgomery & Dietrich, 1992; Sassolas-Serrayat et al., 2018; Dodds & Rothman, 2000).

The average drainage area of nested, space-filling basins stopped growing at a relatively early stage ($T/T_{\text{main divide formation}} \sim 0.6$) of the experiment and simulations (200 x 50 km^2) and then it decreased (Figure 12a). Nested basins Hack's exponent and coefficient was observed to be approximately constant through time, with mostly anomalous values, beyond the range of reported natural values (Hack, 1957;

Montgomery & Dietrich, 1992; Sassolas-Serrayat et al., 2018; Dodds & Rothman, 2000) (Figure 12b and c).

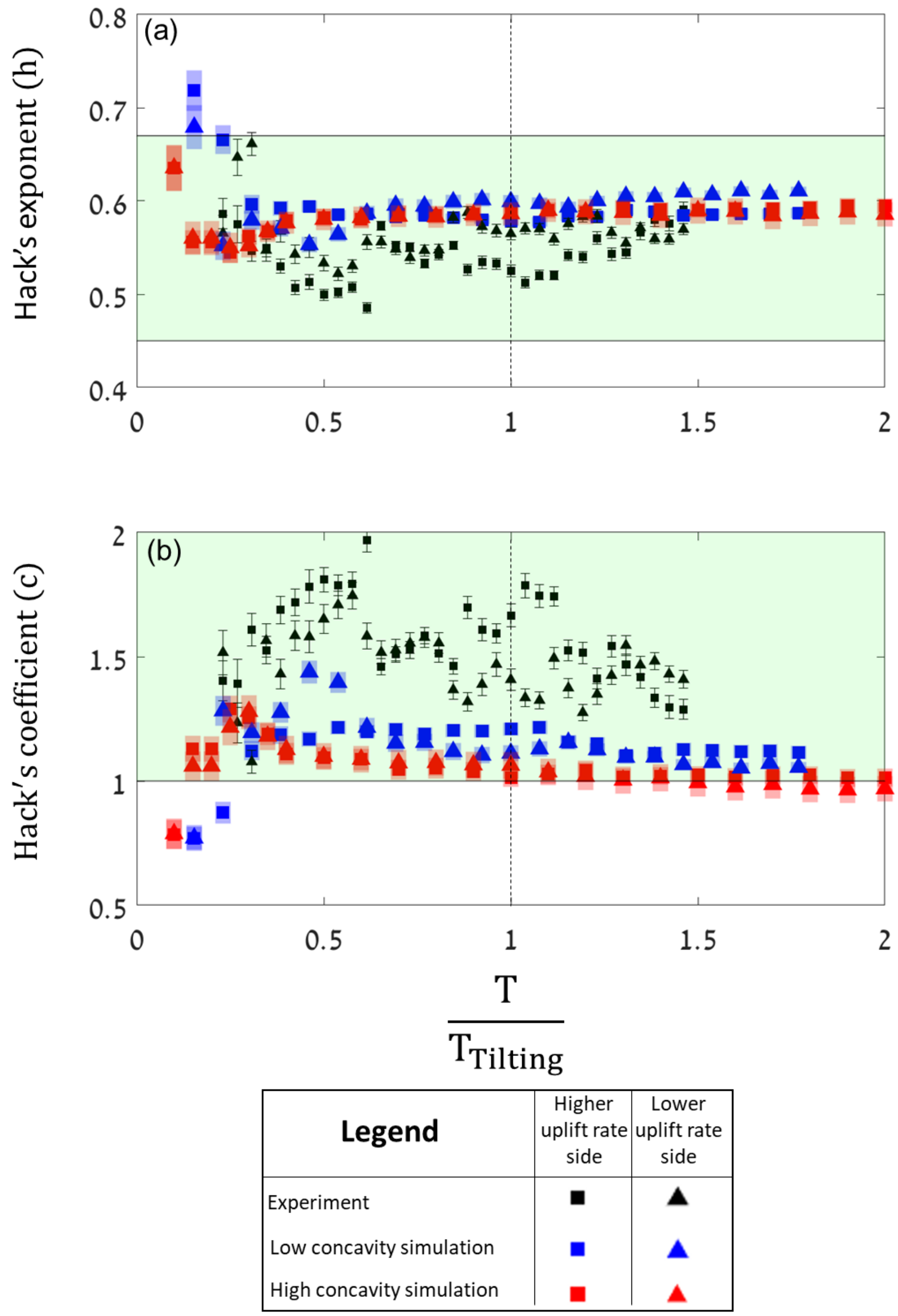

Figure 11: Temporal evolution of (a) Hack's exponent and (b) Hack's coefficient of main basins on the higher (squares) and lower (triangles) uplift rate sides of the landscapes during uniform and differential

uplift in the experiment and simulations (200x50 km^2*). Time axes are normalized to the timing of tilting initiation, depicted by the vertical dashed line (*$T / T_{Tilting} = 1$*). Green rectangle represents the range of naturally observed h and c values reported by previous studies (Hack, 1957; Sassolas-Serrayat et al., 2018; Dodds & Rothman, 2000). In both panels, error bars and colored bars represent the corresponding Hack's parameter's standard deviation of the population produced by bootstrapping.*

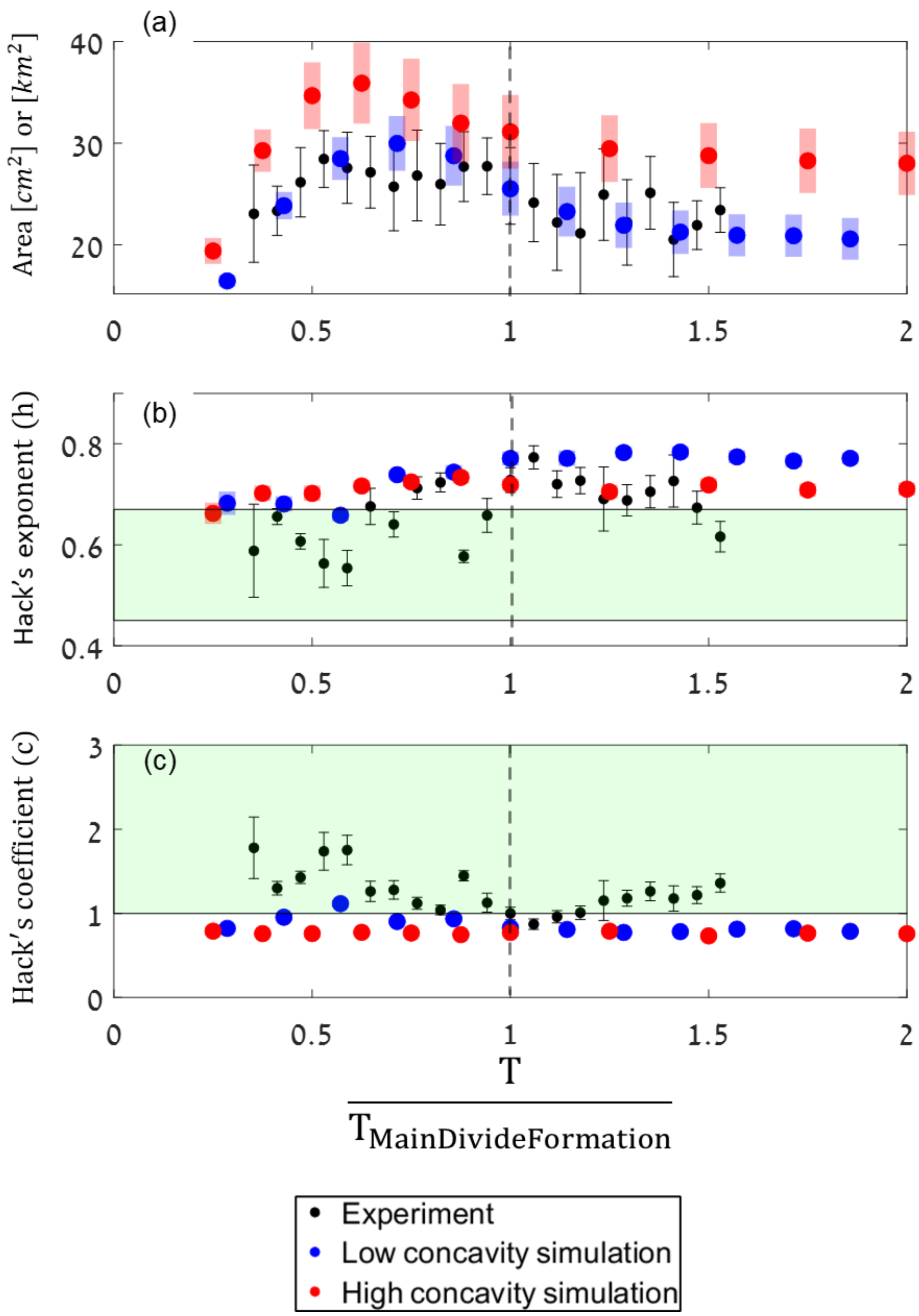

Figure 12: Temporal evolution of (a) average drainage area (b) Hack's exponent and (c) Hack's coefficient of nested basins formed during uniform uplift in the experiment and simulations (200 x 50 km²). Time axes are normalized to the timing of main divide formation, depicted by the vertical dashed black line ($T / T_{MainDivideFormation} = 1$). Green rectangles represent the ranges of naturally inferred h and

c values reported by previous studies (Hack, 1957; Sassolas-Serrayat et al., 2018; Dodds & Rothman, 2000). Error bars and colored bars in (a) represent the standard error (SE) on drainage area and in (b) and (c) the corresponding Hack's parameter's standard deviation of the population produced by bootstrapping.

4. Discussion

4.1. Geometry preserving mechanisms

We performed experiment and simulations to explore the regularity of basins geometry during the evolution of an uplifted terrain in two settings – (1) the emergence of topography and development of a drainage network under uniform uplift, and (2) basin size changes caused by main divide migration due to tilting. In the first setting, the globally consistent spacing ratio and Hack's law parameters of main basins (Hack, 1957; Montgomery & Dietrich, 1992; Sassolas-Serrayat et al., 2018; Dodds & Rothman, 2000; Hovius, 1996; Talling et al., 1997) formed at the onset of drainage development. The preservation of the spacing ratio was achieved by basins' simultaneous sideways expansion and elongation as channels incised the uplifting plateau, in resemblance to the hypothesis proposed by Talling et al. (1997). Sideways expansion truncated the growth of neighboring basins, preventing them from growing and occasionally shrinking their area by processes of beheading. This differential growth decreased the number of main basins (Figure 4) and increased basin spacing (Figure 10b). Consequently, together with basin elongation (Figure 10a), the spacing ratio changed only slightly and remained within the reported range for natural uplifted blocks (Figure 10c).

The rates at which D and S increased were constant during the plateau incision stage in both the experiment and simulations. Essentially, the spacing between basins outlets can be viewed as the width of basins (Hovius, 1996; Talling et al., 1997; Shelef, 2018), so the spacing ratio can also be referred to as the aspect ratio of basins (Shelef, 2018). Therefore, basins must elongate and widen by the same proportion in order to maintain a steady spacing ratio during drainage evolution. Since R in the initial stages of drainage evolution was found to be around two, in order to maintain a value roughly between two and three, the rate of basins widening should equal approximately 1/3 to 1/2 of the rate of basins elongation (Hovius, 1996). These ratios were achieved in both the experiment and simulations: the rates of basin widening were ~0.30 to ~0.46 of the rate of basin elongation.

In the second, tectonic tilting stage, the tectonically induced main divide migration caused basins' size changes. Yet, the geometrical scaling relations remained within the reported narrow range of natural landscapes values. In the experiment and simulations, we did not observe the splitting of basins on the shrinking side that would contribute to maintaining a relatively constant R, as was reported by Bonnet (2009). Instead, along the shrinking side, the average spacing between basins decreased due to the merging of triple divide junctions with the main divide, increasing the number of main basins and decreasing their spacing. On the opposite, elongating side, we observed a counter behavior where main basins disconnected from the main divide, forming new triple divide junctions and causing the average spacing to increase. Similar dynamics were observed in numerical landscapes following main divide migration inflicted by an erodibility gradient (Giachetta et al., 2014). The disconnected main basins were initially narrow and showed relatively high channel head χ values (Figure 9), making them vulnerable to capture and beheading. Following their disconnection, triple divide junction migration continued, and most of these basins shrank via the same processes described above (Figure 11b). Ultimately, these processes assisted in preserving a relatively narrow range of spacing ratios on both sides of the main divide.

To explore the applicability of these processes in a natural setting, we examine the Wula-Shan horst in northern China. This terrain experiences relatively uniform climatic and lithologic conditions (He et al., 2019). A spatial uplift gradient has been suggested to generate a topographically asymmetric block with the main drainage divide positioned closer to the higher uplift rate side, at the southern flank (Figure 13) (He et al., 2019, 2020). Recent studies have argued that the uplift rate gradient between the two flanks decreased, resulting in main divide migration back toward the center of the domain (He et al., 2019, 2021). An analysis of Wula-Shan basins reveals that a few nested basins on the higher uplift rate side appear to have possibly been disconnected from the main divide (Figure 13) as it migrated back toward the center of the domain, and main basins that are susceptible to disconnection if main divide migration persists. χ' analysis that incorporates the currently suggested spatial uplift gradient (He et al., 2019) shows the vulnerability of these basins to reorganization by beheading and capture (Figure 13). On the lower uplift rate side of the Wula-Shan, nested basins whose headwaters are relatively close to the main divide could become incorporated into the main divide if main divide migration persists northward (Figure 13).

The nested basins in our numerical and experimental landscapes are basins that lost in the competition for drainage area at a relatively early stage of drainage network evolution. Being so, they are confined between main basins that managed to grow toward a potentially stable shape (Rigon et al., 1998; Hunt, 2016), indicated by their Hack's parameters that are well within the documented range in nature. Hack's parameters of these nested basins have been shown to be anomalous in natural landscapes, and the shapes of these basins were shown to be relatively narrow (Beeson et al., 2016) and thus prone to losing drainage area to their larger neighboring basins. The anomalous values of nested basins' Hack's parameters computed here (Figure 12a) and in Beeson et al. (2016) indicate that the nested basins probably do not obey the same geometrical scaling relations as the main basins. The ongoing variability in nested basins Hack's parameters observed, may indicate that these basins, which passively fill the space between main basins, act as "drainage area repositories". I.e., when main basins have enough erosive power to grow and increase their area, the nested basins supply the demand with "easy to capture" drainage area.

4.2. Possible relation between *R*, θ, and Hack's parameters

Although the spacing ratios of the experimental and numerical landscapes remained within the narrow range of naturally observed values, consistent differences between the measured values in the simulations are apparent, which could be related to differences in channel concavity. A geometric model proposed by Shelef (2018) referred to this correlation and revealed that in a similar geometric domain, basins' spacing ratio (R), channel concavity (θ), and Hack's exponent (h) are inter-dependent despite them often being measured independently. According to Shelef's model, higher concavities produce lower spacing ratios, as supported also by the simulations presented here (Figure 10c). Essentially, lower concavity channels generate simpler-looking, narrower basin shapes (Shelef & Hilley, 2014), which directly affect the spacing ratio.

Despite the link between Hack's law and spacing ratio (Hovius, 1996; Walcott & Summerfield, 2009), our simulation results show that different channel concavities (θ) share approximately the same Hack's exponent (Figure 11a). This observation indicates that in the numerical landscapes, *R* likely co-varies with θ, while *h* remains more consistent (Shelef, 2018). Hack's coefficient, however, appears more sensitive to the spacing ratio. We observed that a relatively high *R* (and low θ) corresponds to a higher average *c*, as can be seen in Figure 10c andFigure 11b. The same effect is observed in response to tilting, where *R* slightly decreased on the higher uplift rate side (Figure 10c), corresponding to a slight decrease in *c* (Figure 13c) within the same basin group. *R* and *c* co-variance is consistent with the inferences that under the assumption of rectangular basins and a very low channel sinuosity, *c* would be equivalent to the square root of *R* (Hovius, 1996). Further, In accordance with attempts to relate geometrical scaling relations, e.g., Hack's law, to the shape of basins (Sassolas-Serrayat et al., 2018), an increase in *c* of a basin correlates to a basin's elongation, and a decrease correlates to a basin becoming more circular. In agreement with this hypothesis, a co-variant decrease of *c* and *R* is reflected in the observation that basins become more circular as they shorten on the higher uplift rate side.

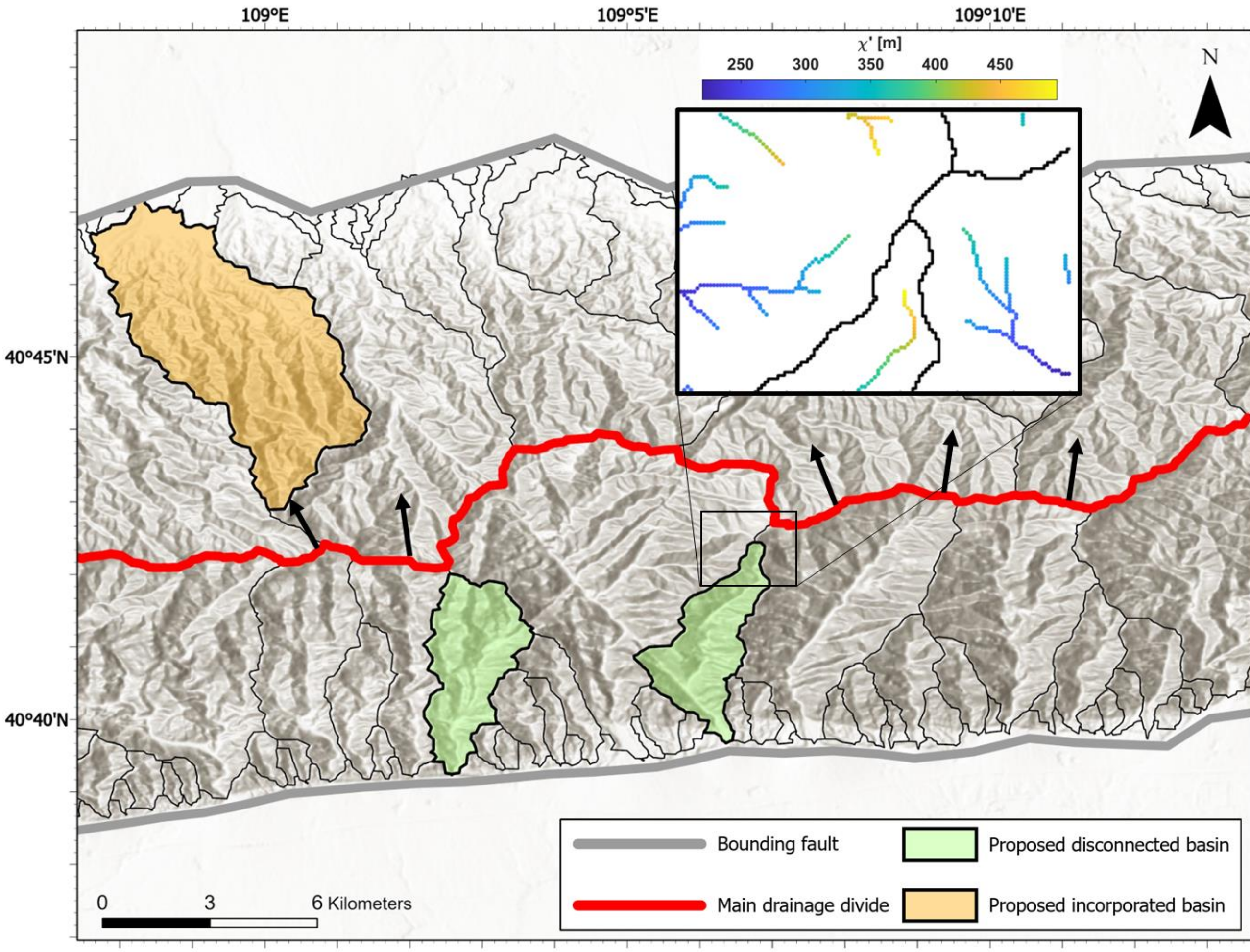

Figure 13: Hill-shade map with delineated drainage basins in the Wula-Shan horst, Northern China. Grey lines depict the bounding faults. The southern fault is uplifting faster than the northern fault, resulting in an asymmetric topography (He et al., 2019, 2021), with the main divide (red line) closer to the south, higher uplift rate edge. He et al. (2019) suggested a recent decrease in uplift gradient between the two faults, causing the main divide to migrate northward. Green-colored basins depict possibly disconnected basins, and the orange-colored basin depicts a basin that could be incorporated into the main divide if its northward migration continues. The inset shows χ' map in the vicinity of a suggested

disconnected basin, assuming the uplift gradient suggested in He et al. (2019). The observed across divide χ' differences could indicate local divide instability and a potentially ongoing beheading or capture that will further shrink the disconnected basin.

4.3. Main drainage divide migration

When climatic, lithologic, and tectonic conditions are uniform and constant during the evolution of an uplifted block, the main divide is expected to emerge at the center of the domain, as has been also observed in experiments (Crave et al., 2000; Lague et al., 2003; Reinhardt & Ellis, 2015) and numerical simulations (Goren et al., 2014; Whipple et al., 2017; He et al., 2021; Shi et al., 2021). However, external perturbations, such as tilting (e.g., Figure 2b), perturb the system. Channels experiencing a greater uplift gradient become steeper, and steady state elevation will be achieved over shorter distances in the higher uplift rate side compared to the lower uplift rate side, resulting in main divide migration toward the higher uplift rate side, overall generating an asymmetric topography (Goren et al., 2014; He et al., 2021). Tectonically induced main divide migration has been observed in numerical simulations (Goren et al., 2014; Whipple et al., 2017; He et al., 2021; Shi et al., 2021) and inferred in natural landscapes (He et al., 2019; Su et al., 2020; Shikakura et al., 2012; Forte et al., 2015), yet, to the best of our knowledge, this work is the first to show this process in an experimental landscape.

4.4. Simulating experimental landscapes

The parameters of the low concavity simulation were chosen to facilitate comparison with the experiment, and the parameters of the high concavity simulation were chosen to simulate a more natural topography. Qualitatively, we observed that basin dynamics in response to the double-stage tectonic scenario were similar in the experiment and simulations. These dynamics include the reorganization associated with differential growth during the uniform uplift stage and the reorganization and main divide migration in response to tilting. Quantitively, considering the scaling factors presented in Section 2.2.2.

(L_0, T_0 and U_0), we can compare process rates between the experimental and numerical landscapes. For example, the experiment and low concavity simulation displayed similar rates of drainage basins growth by elongation and widening (Figure 10a, 10b). In addition, the timing of main divide formation and the average distance of tectonically induced main divide migration appear to be similar between these landscapes (Figure 6). However, the high concavity simulation, displayed a slightly higher rate of basins' growth. Hence, the main divide formed faster.

The substantial similarities in basin-scale processes and rates of landscape response to tectonic perturbations between experimental and numerical landscapes could be interpreted in two ways. First, the observed processes are universal and independent of the dominant erosional mechanism. Therefore, they are likely to occur also in natural landscapes. Second, the dominant emergent fluvial erosion process that acts on the experimental landscapes produced by DULAB could be represented by the stream power incision model that is implemented into the numerical landscapes in DAC. Regardless of the exact interpretation, the observation that channelization reached very close to the water divides in the experiment could indicate that fluvial processes are essential and possibly dominate in controlling the mountain range-scale reorganizational response to changing boundary conditions.

5. Conclusions

The dynamic, plan-view response of drainage basins to changes in tectonic gradients are explored using a newly designed experimental landscape evolution apparatus (DULAB) and a landscape evolution numerical model (DAC). We explored two forms of tectonic changes. First, from a subdued topography to a mature mountain range in response to uniform uplift. Second, from uniform to spatial gradients in uplift in the form of tilting. Our findings derived from the analysis presented here indicate that:

1. The globally observed regularity in drainage basins geometry is a fundamental characteristic of juvenile basins and is maintained as basins grow differentially via processes of beheading and stream capture.
2. Differential uplift in the form of tilting exerted on a well-developed landscape triggers drainage reorganization that changes basins' size but preserves their geometry as their geometrical scaling relations remain constricted within a narrow range. An important process that facilitates this preservation during main divide migration is incorporation of new basins to the main divide along the shrinking side of the domain and disconnection of basins along the elongating side.
3. Predictions of the χ' metric, which incorporates information about the spatial gradients of uplift are consistent with observed changes in drainage topology and divide migration directions.
4. The dynamic response to changes in rock uplift shows significant similarities between the experiment and simulations, providing support that either such a response is process-independent or that experimental landscapes generated using the DULAB apparatus erode with accordance to the stream power incision model. Finally, we found that numerical models, such as DAC, can properly represent landscape evolution at the laboratory scale.

Acknowledgements

Chris Ellis, Chris Paola, Efi Foufoula-Georgiou, and Stephane Bonnet are thanked for valuable discussions and advice that helped us design DULAB. Aharon Tabibian and the BGU Faculty of Natural Sciences workshop are thanked for constructing the DULAB apparatus. Raz Edut is thanked for his invaluable contribution in assembling and maintaining DULAB. Omri Ofri, Yuval Eshet, Tom Kaholi, Hagar Tevet, Guy Fisch and Asher Perry Kellum are thanked for their dedication and hard work in the lab and for their assistance in preforming data analyses. We thank Eitan Shelef for providing insightful comments on an earlier version of the manuscript. This research was funded by the Israel Science

Foundation (ISF grant No. 562/19). Kobi Havusha received support from the Fay and Bert Harbour scholarship. Ron Nativ received support from the Ben-Gurion University of the Negev “high-tech, bio-tech and chemo-tech” scholarship.

Data availability statement

The raw data used in the analysis of the experiment and simulations referred to in this paper, containing DEMs and MATLAB scripts, can be found in the Zenodo data repository with the DOI: 10.5281/zenodo.6890372.

6. References

Bata, A. (2006). "Substrate Control on the Geometry of an Experimental Bedrock Channel." *University of Cambridge*, Cambridge, United Kingdom. Part III Research Project.

Beeson, H. W., & McCoy, S. W. (2020). Geomorphic signatures of the transient fluvial response to tilting. *Earth Surface Dynamics*, *8*(1), 123-159. https://doi.org/10.5194/esurf-8-123-2020

Beeson, H. W., McCoy, S. W., & Willett, S. D., (2016). From shoestring rills to dendritic river networks: Documenting the evolution of river basins towards geometric similarity through divide migration, stream capture and lateral branching: Abstract EP52A-04. Oral session presented at AGU Fall Meeting, San Francisco, CA, 12-16 December.

Bonnet, S. (2009). Shrinking and splitting of drainage basins in orogenic landscapes from the migration of the main drainage divide. *Nature Geoscience*, *2*(11), 766-771. https://doi-org.ezproxy.bgu.ac.il/10.1038/ngeo700

Bonnet, S., & Crave, A. (2003). Landscape response to climate change: Insights from experimental modeling and implications for tectonic versus climatic uplift of topography. *Geology*, *31*(2), 123-126. https://doi.org/10.1130/0091-7613(2003)031<0123:LRTCCI>2.0.CO;2

Bonnet, S., & Crave, A. (2006). Macroscale dynamics of experimental landscapes. *Geological Society, London, Special Publications*, *253*(1), 327-339. https://doi.org/10.1144/GSL.SP.2006.253.01.17

Burbank, D. W., Leland, J., Fielding, E., Anderson, R. S., Brozovic, N., Reid, M. R., & Duncan, C. (1996). Bedrock incision, rock uplift and threshold hillslopes in the northwestern Himalayas. *Nature*, *379*(6565), 505-510. https://doi.org/10.1038/379505a0

Capolongo, D., Giachetta, E., & Refice, A. (2011). Numerical framework for geomorphological experiments. *Geografia Fisica e Dinamica Quaternaria*, *34*, 75-80. https://doi.org/10.4461/GFDQ.2011.34.8

Castelltort, S., & Simpson, G. (2006). River spacing and drainage network growth in widening mountain ranges. *Basin Research*, *18*(3), 267-276. https://doi.org/10.1111/j.1365-2117.2006.00293.x

Castelltort, S., Simpson, G., & Darrioulat, A. (2009). Slope-control on the aspect ratio of river basins. *Terra Nova*, *21*(4), 265-270. https://doi.org/10.1111/j.1365-3121.2009.00880.x

Castelltort, S., Goren, L., Willett, S. D., Champagnac, J. D., Herman, F., & Braun, J. (2012). River drainage patterns in the New Zealand Alps primarily controlled by plate tectonic strain. *Nature Geoscience*, *5*(10), 744-748. https://doi.org/10.1038/ngeo1582

Cheraghi, M., Rinaldo, A., Sander, G. C., Perona, P., & Barry, D. A. (2018). Catchment drainage network scaling laws found experimentally in overland flow morphologies. *Geophysical Research Letters*, *45*(18), 9614-9622. https://doi.org/10.1029/2018GL078351

Cox, S. E., Thomson, S. N., Reiners, P. W., Hemming, S. R., & Van De Flierdt, T. (2010). Extremely low long-term erosion rates around the Gamburtsev Mountains in interior East Antarctica. *Geophysical Research Letters*, *37*(22). https://doi.org/10.1029/2010GL045106

Crave, A., Lague, D., Davy, P., Kermarrec, J., Sokoutis, D., Bodet, L., & Compagnon, R. (2000). Analogue modelling of relief dynamics. *Physics and chemistry of the Earth, part A: Solid Earth and Geodesy*, *25*(6-7), 549-553. https://doi.org/10.1016/S1464-1895(00)00084-3

Densmore, A. L., Dawers, N. H., Gupta, S., & Guidon, R. (2005). What sets topographic relief in extensional footwalls?. *Geology*, *33*(6), 453-456. https://doi.org/10.1130/G21440.1

Dodds, P. S., & Rothman, D. H. (2000). Scaling, universality, and geomorphology. *Annual Review of Earth and Planetary Sciences*, *28*(1), 571-610. https://doi.org/10.1146/annurev.earth.28.1.571

Ellis, M. A., Densmore, A. L., & Anderson, R. S. (1999). Development of mountainous topography in the Basin Ranges, USA. *Basin Research*, *11*(1), 21-42. https://doi.org/10.1046/j.1365-2117.1999.00087.x

Farías, M., Charrier, R., Comte, D., Martinod, J., & Hérail, G. (2005). Late Cenozoic deformation and uplift of the western flank of the Altiplano: Evidence from the depositional, tectonic, and geomorphologic evolution and shallow seismic activity (northern Chile at 19 30′ S). Tectonics, 24(4). https://doi.org/10.1029/2004TC001667

Forte, A. M., & Whipple, K. X. (2018). Criteria and tools for determining drainage divide stability. Earth and Planetary Science Letters, 493, 102-117. https://doi.org/10.1016/j.epsl.2018.04.026

Forte, A. M., Whipple, K. X., & Cowgill, E. (2015). Drainage network reveals patterns and history of active deformation in the eastern Greater Caucasus. *Geosphere*, *11*(5), 1343-1364. https://doi.org/10.1130/GES01121.1

Goren, L., Willett, S. D., Herman, F., & Braun, J. (2014). Coupled numerical–analytical approach to landscape evolution modeling. *Earth Surface Processes and Landforms*, *39*(4), 522-545. https://doi.org/10.1002/esp.3514

Graveleau, F., Hurtrez, J. E., Dominguez, S., & Malavieille, J. (2011). A new experimental material for modeling relief dynamics and interactions between tectonics and surface processes. *Tectonophysics*, *513*(1-4), 68-87. https://doi.org/10.1016/j.tecto.2011.09.029

Guerit, L., Goren, L., Dominguez, S., Malavieille, J., & Castelltort, S. (2018). Landscape ‘stress’ and reorganization from χ-maps: Insights from experimental drainage networks in oblique collision setting. *Earth Surface Processes and Landforms*, *43*(15), 3152-3163. https://doi.org/10.1002/esp.4477

Hack, J. T. (1957). *Studies of longitudinal stream profiles in Virginia and Maryland* (Vol. 294). US Government Printing Office. https://doi.org/10.3133/pp294B

Hasbargen, L. E., & Paola, C. (2000). Landscape instability in an experimental drainage basin. *Geology*, *28*(12), 1067-1070. https://doi.org/10.1130/0091-7613(2000)28<1067:LIIAED>2.0.CO;2

Hasbargen, L. E., & Paola, C. (2003). How predictable is local erosion rate in eroding landscapes?. *GEOPHYSICAL MONOGRAPH-AMERICAN GEOPHYSICAL UNION*, *135*, 231-240. https://doi.org/10.1029/135GM16

He, C., Rao, G., Yang, R., Hu, J., Yao, Q., & Yang, C. J. (2019). Divide migration in response to asymmetric uplift: Insights from the Wula Shan horst, North China. *Geomorphology*, *339*, 44-57. https://doi.org/10.1016/j.geomorph.2019.04.024

He, C., Yang, C. J., Turowski, J. M., Rao, G., Roda-Boluda, D. C., & Yuan, X. P. (2021). Constraining tectonic uplift and advection from the main drainage divide of a mountain belt. *Nature communications*, *12*(1), 1-10. https://doi.org/10.1038/s41467-020-20748-2

Horton, R. E. (1945). Erosional development of streams and their drainage basins; hydrophysical approach to quantitative morphology. *Geological society of America bulletin*, *56*(3), 275-370. https://doi.org/10.1130/0016-7606(1945)56[275:EDOSAT]2.0.CO;2

Hovius, N. (1996). Regular spacing of drainage outlets from linear mountain belts. *Basin Research*, *8*(1), 29-44. https://doi.org/10.1111/j.1365-2117.1996.tb00113.x

Howard, A. D., Dietrich, W. E., & Seidl, M. A. (1994). Modeling fluvial erosion on regional to continental scales. *Journal of Geophysical Research: Solid Earth*, *99*(B7), 13971-13986. https://doi.org/10.1029/94JB00744

Hunt, A. G. (2016). Brief communication: Possible explanation of the values of Hack's drainage basin, river length scaling exponent. *Nonlinear Processes in Geophysics*, *23*(2), 91-93. https://doi.org/10.5194/npg-23-91-2016

Jackson, J., Van Dissen, R., & Berryman, K. (1998). Tilting of active folds and faults in the Manawatu region, New Zealand: evidence from surface drainage patterns. New Zealand Journal of Geology and Geophysics, 41(4), 377-385. https://doi.org/10.1080/00288306.1998.9514817

Lague, D., Crave, A., & Davy, P. (2003). Laboratory experiments simulating the geomorphic response to tectonic uplift. *Journal of Geophysical Research: Solid Earth*, *108*(B1), ETG-3. https://doi.org/10.1029/2002JB001785

Liu, L., & Gurnis, M. (2010). Dynamic subsidence and uplift of the Colorado Plateau. Geology, 38(7), 663-666. https://doi.org/10.1130/G30624.1

Matmon, A., Bierman, P. R., Larsen, J., Southworth, S., Pavich, M., Finkel, R., & Caffee, M. (2003). Erosion of an ancient mountain range, the Great Smoky Mountains, North Carolina and Tennessee. *American Journal of Science*, *303*(9), 817-855. https://doi.org/10.2475/ajs.303.9.817

McMillan, M. E., Angevine, C. L., & Heller, P. L. (2002). Postdepositional tilt of the Miocene-Pliocene Ogallala Group on the western Great Plains: Evidence of late Cenozoic uplift of the Rocky Mountains. Geology, 30(1), 63-66. https://doi.org/10.1130/0091-7613(2002)030<0063:PTOTMP>2.0.CO;2

Montgomery, D. R., & Brandon, M. T. (2002). Topographic controls on erosion rates in tectonically active mountain ranges. *Earth and Planetary Science Letters*, *201*(3-4), 481-489. https://doi.org/10.1016/S0012-821X(02)00725-2

Montgomery, D. R., & Dietrich, W. E. (1992). Channel initiation and the problem of landscape scale. *Science*, *255*(5046), 826-830. https://doi.org/10.1126/science.255.5046.826

Mueller, J. E. (1973). Re-evaluation of the relationship of master streams and drainage basins: Reply. *Geological Society of America Bulletin*, *84*(9), 3127-3130. https://doi.org/10.1130/0016-7606(1973)84<3127:ROTROM>2.0.CO;2

Paola, C., Straub, K., Mohrig, D., & Reinhardt, L. (2009). The “unreasonable effectiveness” of stratigraphic and geomorphic experiments. *Earth-Science Reviews*, *97*(1-4), 1-43. https://doi.org/10.1016/j.earscirev.2009.05.003

Perron, J. T., & Royden, L. (2013). An integral approach to bedrock river profile analysis. *Earth Surface Processes and Landforms*, *38*(6), 570-576. https://doi.org/10.1002/esp.3302

Purdie, H., & Brook, M. (2006). Drainage spacing regularity on a fault-block: A case study from the eastern Ruahine Range. *New Zealand Geographer*, *62*(2), 97-104. https://doi.org/10.1111/j.1745-7939.2006.00034.x

Reinhardt, L., & Ellis, M. A. (2015). The emergence of topographic steady state in a perpetually dynamic self-organized critical landscape. *Water Resources Research*, *51*(7), 4986-5003. https://doi.org/10.1002/2014WR016223

Reitano, R., Faccenna, C., Funiciello, F., Corbi, F., & Willett, S. D. (2020). Erosional response of granular material in landscape models. *Earth Surface Dynamics*, *8*(4), 973-993. https://doi.org/10.5194/esurf-8-973-2020

Rigon, R., Rodriguez-Iturbe, I., & Rinaldo, A. (1998). Feasible optimality implies Hack's law. *Water resources research*, *34*(11), 3181-3189. https://doi.org/10.1029/98WR02287

Sassolas-Serrayet, T., Cattin, R., & Ferry, M. (2018). The shape of watersheds. *Nature communications*, *9*(1), 1-8. https://doi.org/10.1038/s41467-018-06210-4

Scherler, D., & Schwanghart, W. (2020a). Drainage divide networks–Part 1: Identification and ordering in digital elevation models. *Earth Surface Dynamics*, *8*(2), 245-259. https://doi.org/10.5194/esurf-8-245-2020

Scherler, D., & Schwanghart, W. (2020b). Drainage divide networks–Part 2: Response to perturbations. *Earth Surface Dynamics*, *8*(2), 261-274. https://doi.org/10.5194/esurf-8-261-2020

Schwanghart, W., & Scherler, D. (2014). TopoToolbox 2–MATLAB-based software for topographic analysis and modeling in Earth surface sciences. Earth Surface Dynamics, 2(1), 1-7. https://doi.org/10.5194/esurf-2-1-2014

Shelef, E. (2018). Channel Profile and Plan-View Controls on the Aspect Ratio of River Basins. *Geophysical Research Letters*, *45*(21), 11-712. https://doi.org/10.1029/2018GL080172

Shelef, E., & Hilley, G. E. (2014). Symmetry, randomness, and process in the structure of branched channel networks. *Geophysical Research Letters*, *41*(10), 3485-3493. https://doi.org/10.1002/2014GL059816

Shi, F., Tan, X., Zhou, C., & Liu, Y. (2021). Impact of asymmetric uplift on mountain asymmetry: Analytical solution, numerical modeling, and natural examples. *Geomorphology*, 107862. https://doi.org/10.1016/j.geomorph.2021.107862

Shikakura, Y., Fukahata, Y., & Matsu'ura, M. (2012). Spatial relationship between topography and rock uplift patterns in asymmetric mountain ranges based on a stream erosion model. *Geomorphology*, *138*(1), 162-170. https://doi.org/10.1016/j.geomorph.2011.09.002

Shreve, R. L. (1966). Statistical law of stream numbers. *The Journal of Geology*, *74*(1), 17-37. https://doi.org/10.1086/627137

Stockli, D. F., Dumitru, T. A., McWilliams, M. O., & Farley, K. A. (2003). Cenozoic tectonic evolution of the White Mountains, California and Nevada. Geological Society of America Bulletin, 115(7), 788-816. https://doi.org/10.1130/0016-7606(2003)115<0788:CTEOTW>2.0.CO;2

Strahler, A. (1964). Quantitative Geomorphology of Drainage Basins and Channel Networks. In: Chow, V., Ed., Handbook of Applied Hydrology, McGraw Hill, New York, 439-476.

Su, Q., Wang, X., Lu, H., & Xie, H. (2020). Dynamic Divide Migration as a Response to Asymmetric Uplift: An Example from the Zhongtiao Shan, North China. Remote Sensing, 12(24), 4188. https://doi.org/10.3390/rs12244188

Sweeney, K. E., Roering, J. J., & Ellis, C. (2015). Experimental evidence for hillslope control of landscape scale. *Science*, *349*(6243), 51-53. https://doi.org/10.1126/science.aab0017

Talling, P. J., Stewart, M. D., Stark, C. P., Gupta, S., & Vincent, S. J. (1997). Regular spacing of drainage outlets from linear fault blocks. *Basin research*, *9*(4), 275-302. https://doi.org/10.1046/j.1365-2117.1997.00048.x

Tucker, G. E., & Whipple, K. X. (2002). Topographic outcomes predicted by stream erosion models: Sensitivity analysis and intermodel comparison. Journal of Geophysical Research: Solid Earth, 107(B9), ETG-1. https://doi.org/10.1029/2000JB000044

Walcott, R. C., & Summerfield, M. A. (2009). "Universality and variability in basin outlet spacing: implications for the two-dimensional form of drainage basins." *Basin Research* 21.2: 147-155. https://doi.org/10.1111/j.1365-2117.2008.00379.x

Whipple, K. X., & Tucker, G. E. (1999). Dynamics of the stream-power river incision model: Implications for height limits of mountain ranges, landscape response timescales, and research needs. *Journal of Geophysical Research: Solid Earth*, *104*(B8), 17661-17674. https://doi.org/10.1029/1999JB900120

Whipple, K. X., Forte, A. M., DiBiase, R. A., Gasparini, N. M., & Ouimet, W. B. (2017). Timescales of landscape response to divide migration and drainage capture: Implications for the role of divide mobility in landscape evolution. *Journal of Geophysical Research: Earth Surface*, *122*(1), 248-273. https://doi.org/10.1002/2016JF003973

Whittaker, A. C., Attal, M., Cowie, P. A., Tucker, G. E., & Roberts, G. (2008). Decoding temporal and spatial patterns of fault uplift using transient river long profiles. *Geomorphology*, *100*(3-4), 506-526. https://doi.org/10.1016/j.geomorph.2008.01.018

Willemin, J. H. (2000). Hack's law: Sinuosity, convexity, elongation. *Water Resources Research*, *36*(11), 3365-3374. https://doi.org/10.1029/2000WR900229

Willett, S. D. (2010). Erosion on a line. *Tectonophysics*, *484*(1-4), 168-180. https://doi.org/10.1016/j.tecto.2009.09.011

Willett, S. D., McCoy, S. W., Perron, J. T., Goren, L., & Chen, C. Y. (2014). Dynamic reorganization of river basins. *Science, 343*(6175). https://doi.org/10.1126/science.1248765